

CLOUD: A Scalable and Physics-Informed Foundation Model for Crystal Representation Learning

Changwen Xu¹, Shang Zhu¹, Venkatasubramanian Viswanathan^{1,2*}

¹Department of Mechanical Engineering, University of Michigan.

²Department of Aerospace Engineering, University of Michigan.

*Corresponding author(s). E-mail(s): venkvis@umich.edu;
Contributing authors: changwex@umich.edu; shangzhu@umich.edu;

Abstract

The prediction of crystal properties is essential for understanding structure-property relationships and accelerating the discovery of functional materials. However, conventional approaches relying on experimental measurements or density functional theory (DFT) calculations are often resource-intensive, limiting their scalability. Machine learning (ML) models offer a promising alternative by learning complex structure-property relationships from data, enabling faster predictions. Yet, existing ML models often rely on labeled data, adopt representations that remain limited in capturing essential structural characteristics, and lack integration with physical principles—factors that constrain their generalizability and interpretability. Here, we introduce CLOUD (Crystal Language mOdel for Unified and Differentiable materials modeling), a transformer-based framework trained on a novel Symmetry-Consistent Ordered Parameter Encoding (SCOPE) that encodes crystal symmetry, Wyckoff positions, and composition in a compact, coordinate-free string representation. Pre-trained on over six million crystal structures, CLOUD is fine-tuned on multiple downstream tasks and achieves competitive performance in predicting a wide range of material properties, demonstrating strong scaling performance with respect to data and model size. Furthermore, as a proof of concept of differentiable materials modeling, CLOUD is applied to predict the phonon internal energy and heat capacity, which integrates the Debye model to preserve thermodynamic consistency. This approach enforces thermodynamic consistency and enables temperature-dependent property prediction without requiring additional data, illustrating the broader potential of combining ML with physical laws for materials applications. These results demonstrate the potential of CLOUD as a

scalable and physics-informed foundation model for crystalline materials, unifying symmetry-consistent representations with physically grounded learning for property prediction and materials discovery.

Introduction

Predicting the properties of crystalline materials is of scientific and technological significance, as it enables insight into structure-property relationships and facilitates the discovery of novel functional materials [1–5]. Accurate knowledge of material properties underpins the design of functional materials across a broad range of applications, including electronics [6], energy storage [7, 8], and catalysis [8, 9]. One illustrative example is the heat capacity at constant volume (C_v) which serves as a representative example of a thermodynamic property that plays a key role in vibrational analysis and phase stability [10–12]. As such, the ability to predict these properties from a material’s structure is essential for accelerating the development of new materials and deepening our understanding of structure–property relationships.

Conventionally, crystal properties are evaluated through experimental characterization or theoretical simulations. In the lab, properties such as crystal structure, conductivity, and stability are measured using techniques like X-ray diffraction, spectroscopy, or electrochemical analysis. On the theoretical side, Density Functional Theory (DFT) is widely used to compute formation energies, electronic structures, and elastic constants from first principles. However, these approaches are often time-consuming and resource-intensive, limiting their scalability for high-throughput screening and materials discovery [13, 14]. Consequently, materials development has been constrained to a limited portion of the vast chemical space of synthesizable crystalline materials due to the high costs associated with evaluating material properties within specific systems [15, 16]. To overcome these limitations, the materials science community has increasingly embraced data-driven methods for predicting material properties with high throughput, reducing reliance on costly simulations and resource-intensive experiments. Among these, machine learning surrogates have proven especially effective, as they can learn complex structure-property relationships from data and enable rapid, scalable property predictions. Leveraging these strengths, ML models have the potential to substantially broaden the scope of material performance evaluation in the vast chemical space of crystals [17]. Pioneering work has significantly improved the prediction accuracy for crystals [18–22]. Rational design of representations that map crystals to continuous vector space has enabled the development of more accurate and generalizable machine learning models for crystal property prediction. Early models focused on composition-based representations [20, 23, 24], which are simple and broadly accessible but suffer from limited expressiveness due to their inability to distinguish between structural polymorphs. Structure-based models overcome this limitation by leveraging atomic coordinates, often through graph neural networks, to capture geometric and spatial information [18, 19, 21, 25, 26]. However, these models struggle with long-range interactions [27] and require costly structural data. To

bridge the gap, coordinate-free models have emerged, offering a balance between structural awareness and computational efficiency by encoding symmetry and connectivity without explicit coordinates [28–30]. Nevertheless, current coordinate-free representations still face challenges in efficiently encoding critical structural information for accurate property predictions, motivating the need for improved representations that balance structural richness and computational simplicity.

Despite the advances in material property prediction with machine learning, state-of-the-art (SOTA) models typically rely on labeled training data obtained through costly wet-lab experiments or density functional theory (DFT) calculations. This reliance limits their applicability and scalability due to the scarcity, high cost, and variability of labeled materials datasets [31]. Moreover, these models often exhibit poor out-of-distribution (OOD) generalization, which is critical for real-world applications where crystals with novel compositions or structures are common [17]. Recently, foundation models (FMs) [32], which are trained on broad data at scale and can be adapted to a wide range of downstream tasks, have emerged as a promising solution. Most FMs adopt a transformer-based architecture [33], enabling them to be pre-trained at scale using vast amounts of unlabeled data [34–36], which are orders of magnitude more abundant than labeled data. The key motivation for pre-training on large-scale unlabeled datasets is to learn universal representations of crystals through self-supervised learning. These representations can be effectively transferred to a wide range of downstream tasks, improving model performance even in low-data regimes. Furthermore, the implicit parallelism of attention allows for massively scalable transformer architectures, whose performance can improve predictably with the size of the model and training data, following neural scaling laws [37–39]. If such a scaling behavior holds, FMs are expected to achieve SOTA performance simply by increasing the data and model capacity. FMs leverage self-supervised pretraining to capture high-level structural and chemical patterns from unlabeled data [32, 40], which has shown promise in predicting crystal properties [41–43]. In the molecular domain, models like ChemBERTa [44] and MoLFormer [45] have demonstrated that performance improves with larger pre-training datasets across both regression and classification tasks. Systematic studies on neural scaling laws have been conducted for molecular property prediction [40, 46], yet such analyses remain largely unexplored for materials-focused foundation models.

Another key question of developing foundation models for crystalline materials lies in the incorporation of physics. Even though high predictive accuracy could be achieved with machine-learning models, the prediction consistency in physics is not necessarily guaranteed. For example, previous work [27, 47] that learns the mapping from crystal structures to heat capacity (C_v) in a pure data-driven manner fails to learn the temperature dependency of C_v , hence these models are only capable of predicting C_v values under exactly the same temperature as the training data, which limits their applications in real-world material science tasks. Gurunathan et al. [48] predicted the phonon density of states (pDOS) from which C_v could be calculated with the standard Bose-Einstein distribution formalism, accomplishing enhanced predictive accuracy for temperature-dependent phonon-based properties. However, the model itself is still predicting the target property in one-shot given the input structure

without injecting physics prior. The machine learning model can be further integrated with physical laws by predicting the variables within these laws, which, in turn, determine the target property. This framework can be trained end-to-end, provided that the physical law is differentiable. Recently, DiffMix [49] is developed as a differentiable geometric deep learning framework for mixtures that learns physical coefficients in pre-defined mixture physics laws, showing promising performances than purely data-driven methods, especially in small datasets. DiffMix exhibits strong extrapolation to higher temperatures, enhancing predictive reliability beyond training conditions. By integrating physics-based modeling with geometric deep learning, it enables more accurate and generalizable predictions, supporting efficient material design and optimization. Recent advances in differentiable materials modeling [50–52] have unified physical simulation and learning by enabling gradient-based optimization through physical laws, such as thermodynamic potentials, finite element solvers, or lattice mechanics. These frameworks allow models to predict intermediate physical quantities and propagate gradients through differentiable physical pipelines, supporting data-efficient and generalizable material design.

Herein, we design Symmetry-Consistent Ordered Parameter Encoding (SCOPE) to represent crystal structures as sequences and consequently propose Crystal Language mOdel for Unified and Differentiable materials modeling (CLOUD), a transformer-based foundation model for accurate and generalizable crystal property predictions. The model consists of a BERT [34] encoder and a multi-layer perceptron (MLP) prediction head. SCOPE is a symmetry-consistent string representation for crystals that integrates symmetry, equivalent sites, and compositions in a coordinate-free encoding of the crystal structures, as shown in Figure 1b. Using this representation, CLOUD is pre-trained via masked language modeling (MLM) on $\sim 6.3\text{M}$ unique crystals collected from the OPTIMADE [53], representing one of the largest high-quality datasets of DFT-relaxed crystals to date, then fine-tuned on downstream datasets to learn task-specific structure-property relationships (shown in Figure 1c). CLOUD exhibits competitive model performance when evaluated for predicting various DFT-calculated material properties, indicating its potential as the surrogate model in the loop of material discovery. Additionally, we investigate the scaling performance of CLOUD, suggesting potential performance gains with further scaling of data and model size. We further integrate CLOUD in a differentiable physics framework for physics-consistent property predictions. To showcase this capability, we fuse the model with Debye model [54] (CLOUD-DEBYE, Figure 1d) and assess its ability to predict phonon internal energy and heat capacity, two properties that rely on long-range dependencies of crystal structures. CLOUD-DEBYE exhibits improved predictive performance than CLOUD itself and other GNN or GNN-hybrid models, in the meantime its predictions for the heat capacity under different temperatures match the experimental data and ensure thermodynamic consistency. Such results suggest the potential of CLOUD to learn long-range interactions in crystal structures and observe physics consistency by integrating with physics-based models in materials applications. Overall, our model extends the machine learning models for crystal representation learning and property predictions by developing a novel string representation for effective encoding, building

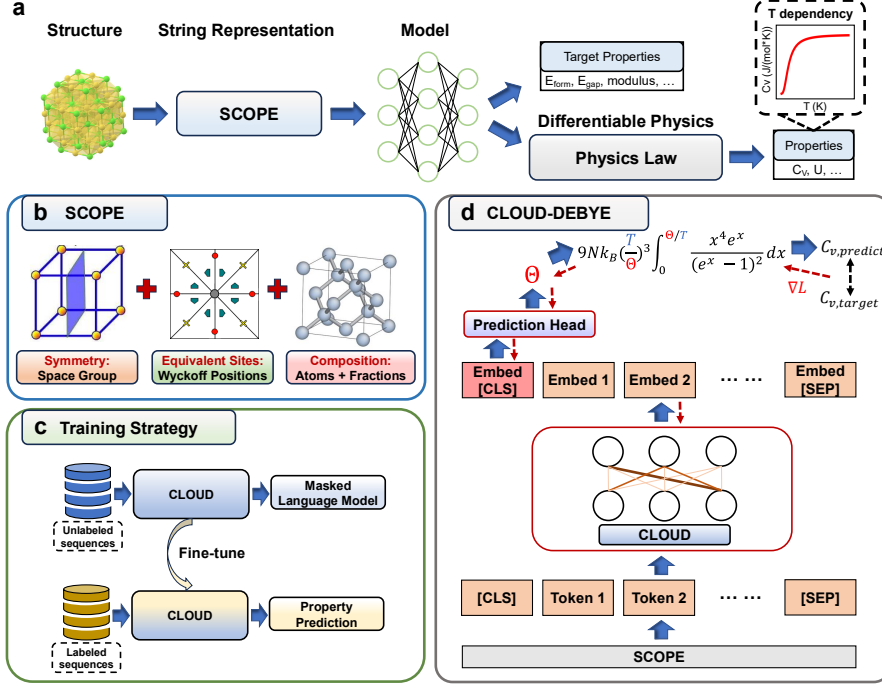


Fig. 1 Overview of CLOUD. **a** For a given crystal structure, we build the string representation SCOPE for it, which will serve as the input of the deep learning model CLOUD which predicts the material properties. Aside from directly outputting the properties of interest, the model can also predict physical variables that fit in known physics laws for physics-consistent property predictions. The three blocks below illustrate the key components of the CLOUD framework. **b** SCOPE representation, a symmetry-consistent string representation for crystal structures, consists of space group generator strings, Wyckoff position symbols, and material composition. **c** Our model CLOUD is pre-trained on million-scale unlabeled data with masked language modeling (MLM) to recover the original tokens, while the feature vector corresponding to token '[CLS]' from the last hidden layer is used for prediction when fine-tuning on diverse downstream tasks (labeled material property data). **d** CLOUD-DEBYE is an example of integrating the foundation model CLOUD and physics laws in a differentiable physics framework. The example exhibits the prediction for constant-volume heat capacity (C_v) where CLOUD outputs the Debye temperature (Θ) and the Debye model predicts C_v using Θ as input under different temperatures. The differentiable implementation of the Debye model enables training the model end-to-end with C_v targets.

an accurate and scalable foundation model, and unifying physics models and data-driven techniques, thus possessing the potential to boost real-world material design and discovery.

Results

Symmetry-Consistent Ordered Parameter Encoding (SCOPE) crystal representation

Crystal representations in machine learning often fall into two broad categories: composition-based and structure-based. Composition-only representations, while easy to obtain, lack the specificity required to uniquely determine a structure due to the non-uniqueness of composition-structure relationships. On the other hand, structure-based graph representations typically rely on 3D atomic coordinates, which are expensive to compute and often unavailable. Moreover, both categories often overlook a fundamental feature of crystals: symmetry, which governs many physical properties such as electronic behavior, optical response, and mechanical stability [55]. To capture symmetry explicitly, many recent models incorporate equivariance constraints [56–58], although these introduce complexity into the architecture. Huang et al. [30] took a step forward by incorporating space group numbers and symbols into a sequence-based representation suitable for language models. However, these symbolic identifiers—such as $P2_1/c$ or #14—are compact summaries rather than full encodings of symmetry operations. They do not convey the complete set of transformations that define the space group, such as mirror plane, rotation axis, or screw axes, nor do they capture the relationship between different space groups.

To address these limitations, we introduce **SCOPE**: a **S**ymmetry-**C**onsistent **O**rdered **P**arameter **E**ncoding. SCOPE is a coordinate-free string representation that integrates three essential components of a crystal structure: the space group, the Wyckoff positions, and the composition. By omitting explicit atomic coordinates and instead encoding symmetry constraints and atomic assignments, SCOPE captures the essential building blocks of a crystal structure in a compact and expressive form.

Symmetry. A crystal structure can be described mathematically by its lattice and basis. Following the notations in Jiao et al. [59], the lattice is a periodic grid in three-dimensional space defined by three linearly independent lattice vectors forming a matrix $\mathbf{L} = [\mathbf{l}_1, \mathbf{l}_2, \mathbf{l}_3] \in \mathbb{R}^{3 \times 3}$. Atomic positions within a unit cell are specified by fractional coordinates $\mathbf{F} = [\mathbf{f}_1, \mathbf{f}_2, \dots, \mathbf{f}_N] \in [0, 1)^{3 \times N}$, which relate to Cartesian coordinates by $\mathbf{X} = \mathbf{L}\mathbf{F}$. A crystal is fully specified by its lattice \mathbf{L} , the set of atomic positions \mathbf{X} , and the chemical species occupying those positions. However, not all configurations are physically meaningful—most crystals exhibit symmetry, which constrains how atoms can be arranged.

The full symmetry of a crystal is captured by its *space group*, a finite set of symmetry operations $g \in G$ that map the crystal onto itself. Each operation acts on the atomic coordinates $\mathbf{X} \in \mathbb{R}^{3 \times N}$ as:

$$g \cdot \mathbf{X} := \mathbf{O}\mathbf{X} + \mathbf{t}\mathbf{1}^\top \quad (1)$$

where $\mathbf{O} \in O(3)$ is an orthogonal matrix representing rotations, reflections, or rotoinversions, and $\mathbf{t} \in \mathbb{R}^3$ is a translation vector. The crystal structure \mathcal{M} is said to be invariant under g if $g \cdot \mathcal{M} = \mathcal{M}$ (here, “=” denotes equivariance under the group action).

Traditionally, space groups are denoted by Hermann–Mauguin symbols or numbers (1–230), which provide compact, human-readable summaries of the symmetry elements. However, these representations are not sufficiently expressive for machine learning—they do not enumerate the full set of symmetry operations or distinguish subtle relationships between different groups.

To overcome this, SCOPE uses *generator strings* [60], which provide a symbolic representation of the symmetry generators for each space group. These generators are a minimal set of operations from which the entire space group can be constructed, allowing for a more granular and interpretable encoding of symmetry.

Among all the possible $g \in G$ in a space group, a *generator* is a fundamental symmetry operator from which all other operations of the space group can be derived through the combination of those basis operators. By selecting a minimal set of generators, we can fully describe the symmetry content of a space group. Therefore, each generator is represented with a symbolic notation to form the generator string for space groups. There are 14 generator matrices for all the symmetry operations besides translational symmetry (namely \mathbf{O} in g), and these matrices are represented by letters ranging from a to n . Combining the generator matrices with the translation components (\mathbf{t} in g) which are represented with 10 upper-case letters, we can obtain all the symmetry operators. With the generators, it is possible to compile all 230 space groups in a short ASCII file that is only 4104 bytes long. The generator strings form a compact representation of all the allowable basic symmetries of the crystal structure, hence making the generator strings *fingerprints* of symmetries. The generator strings are particularly well suited for language modeling, as it preserves the symmetry operations and provides a richer input format than traditional number-based space group identifiers. More information on the generator strings can be found in the Methods section and Section 10.3.6 in De Graef et al. [60].

Equivalent sites. Following the symmetry part, SCOPE encodes the atom positions under the constraints of symmetry. Atom positions are usually represented by atomic coordinates in the form of (x, y, z) in 3D space. However, using coordinate information is computationally intensive in terms of both data acquisition and model training. The acquisition of coordinate information necessitates DFT calculations for structure relaxation, while the model will grow extremely large as the crystal system grows larger. Alternatively, *Wyckoff positions* [28, 61] describe sets of symmetry-equivalent points in the unit cell given space group could be used for atomic position representation. Each Wyckoff position corresponds to a class of points whose *site-symmetry group* is conjugate under G . The site-symmetry group of a point $\mathbf{f}_i \in [0, 1)^3$ is defined as the stabilizer subgroup:

$$G_i = \{g \in G \mid g \cdot \mathbf{f}_i \sim \mathbf{f}_i\}, \quad (2)$$

where $g \cdot \mathbf{f}_i = \mathbf{R}\mathbf{f}_i + \mathbf{t}$, and \sim denotes equivalence under lattice translations. This group contains all symmetry operations that leave the point invariant up to translation.

Applying the full space group G to a representative point \mathbf{f}_i generates a set of symmetry-equivalent positions:

$$\mathcal{W}_i = \{g \cdot \mathbf{f}_i \mid g \in G\}, \quad (3)$$

whose cardinality is called the *multiplicity* of the Wyckoff position. Each Wyckoff position is denoted by a label such as $4d$, where the number indicates the multiplicity $|\mathcal{W}_i|$, and the letter encodes the relative site-symmetry: labels earlier in the alphabet correspond to higher-symmetry positions.

The set of available Wyckoff positions is uniquely determined by the space group, and each atom in a crystal can be assigned to a Wyckoff position according to its symmetry environment. In our SCOPE representation, we encode the occupied Wyckoff positions along with the corresponding chemical elements. This yields a compact and symmetry-consistent description of the crystal structure that is invariant under symmetry-preserving transformations and independent of explicit atomic coordinates.

Composition. We complete the representation by including the elements that make up the material along with their fractions in the material. As a result, the representation is informed of the material’s composition, ensuring that the model captures both the identity and proportion of elements.

Combining the three parts above, we obtain the symmetry-consistent string representation for crystal structures. Examples of representations can be found in Figure 2a. The representation forms a top-down description of the crystal structure – starting from symmetry which is global information of the structure, followed by the equivalent sites under the symmetry and the stoichiometry of the crystal – without explicitly encoding the structure itself, accomplishing efficient encoding of crystals. With the SCOPE representation for crystal structures as the input, we tokenize the sequence so that each chemically meaningful unit is treated as a single token. Specifically, each symbol in the generator string is tokenized individually, each Wyckoff position symbol is treated as a single token, and both element symbols and fractional values are represented as distinct tokens. All the float numbers are rounded to 2 decimal places.

Transferable and scalable crystal representation learning with CLOUD

CLOUD adopts the BERT architecture [34] and follows the pretrain-finetune paradigm for training. The transformer model is based on the attention mechanism [33], enabling it to effectively model long-range dependencies and contextual relationships within sequences. Specifically, it employs scaled dot-product attention, which operates through query, key, and value matrices. Further details on attention are provided in the Methods section. In our implementation, the transformer encoder consists of 12 hidden layers, each comprising 12 attention heads. The hyperparameters of CLOUD are initially set based on standard BERT configurations and subsequently tuned to optimize model performance. The hyperparameters that are experimented with are summarized in Table S1. The transformer encoder is pretrained via Masked Language Modeling (MLM) [62–64] for effective representation learning from the unlabeled

sequences, where 15% of the tokens in a sequence are randomly selected for potential replacement, and the pretraining objective is to reconstruct the original tokens by leveraging contextual information. The pretrained model is subsequently fine-tuned in a supervised manner for crystal property prediction. Specifically, the final hidden states (feature vector) of the special token '[CLS]', positioned at the beginning of the sequence, is passed through the prediction head to generate the prediction output.

We use the Open Databases Integration for Materials Design (OPTIMADE) [53] dataset for CLOUD pre-training. OPTIMADE comprehensively collects crystal data from various databases and provides an API for users with easy access to download the data. We download and de-duplicate the initial ~ 13 M CIF files from OPTIMADE, resulting in ~ 6.3 M data for pre-training. With the pre-trained model, we evaluate the predictive performance of CLOUD on MatBench datasets [65] which comprise diverse materials properties computed via DFT. We compare CLOUD to diverse baseline models in terms of mean absolute error (MAE) normalized by mean absolute deviation (MAD), which is given by $MAE/MAD = \frac{\sum |y_i - y_{i,true}|}{\sum |y_{i,true} - \bar{y}|}$ so that the metric is invariant to scaling, enabling comparison across datasets of different units [21]. The baseline models are primarily divided into three groups: structure-based models which utilize coordinates of atoms as input: CGCNN [19] and ALIGNN [21], structure-agnostic models which do not require structural information: Roost [20], and coordinate-free models which rely on the structures to build the input while do not require the inclusion of atomic coordinates: Wrenformer [66], MatInFormer [30], and SLICES-BERT [29]. CLOUD achieves competitive results across nearly all eight regression tasks compared to structure-agnostic and coordinate-free models. As shown in Figure 2b, CLOUD outperforms previous coordinate-free models in 7 out of 8 tasks and overall performs the best in jdft2d and dielectric datasets. Notably, the model attains strong performance even on data-limited tasks, suggesting that pre-training on large unlabeled datasets enhances generalization. Additionally, CLOUD surpasses MatInFormer [30], indicating that explicit symmetry encoding via generator strings contributes to improved predictive accuracy. Compared to SLICES [29] which encodes bond connectivity while neglecting overall symmetry, CLOUD reaches lower prediction error with much more compact representation (the mean sequence lengths for CLOUD and SLICES are 31 and 513 respectively for the same pre-train dataset), and consequently less computing budgets. SLICES-BERT only surpasses CLOUD on perovskites on which none of the structure-agnostic or coordinate-free models perform well while SLICES benefits from connectivity information which conveys more subtle differences between perovskite structures. We provide the MAE results for each model on the eight regression tasks in Table S3. Figure 2c presents the comparison between the results of CLOUD with/without pre-training. Model performance on downstream tasks is significantly enhanced if the model is pre-trained compared to training from scratch.

Aside from predicting the material properties from the relaxed crystal structures, we are also interested in assessing CLOUD’s capability for structure stability prediction without knowing the relaxed crystal structures from DFT calculations. Therefore, we fine-tune the pre-trained model on MatBench Discovery [66] which is designed to evaluate machine learning models for materials discovery, particularly for predicting

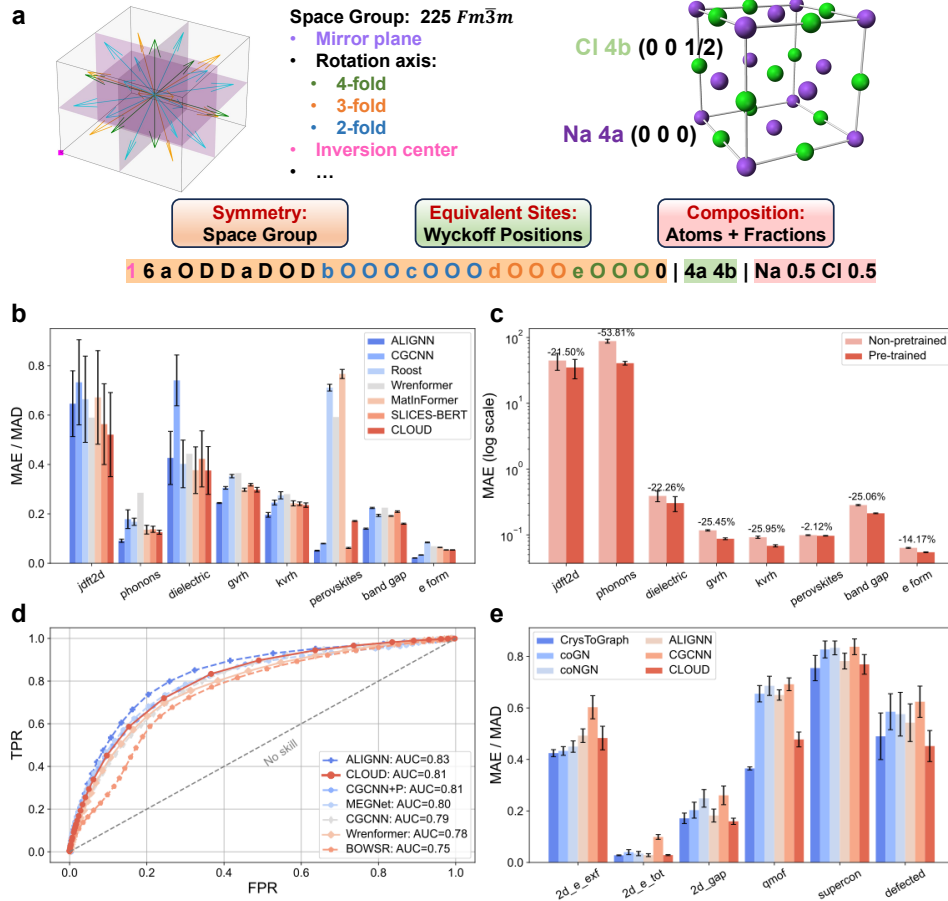


Fig. 2 Illustration of SCOPE representation and fine-tuning results of CLOUD. **a** SCOPE consists of space group generator strings, Wyckoff position symbols, and material compositions. The example of NaCl includes the illustration for space group symmetries and equivalent sites in the unit cell. **b** Fine-tuning results on MatBench regression tasks. All results are shown in the mean of test MAE/MAD in five-fold cross-validation along with the standard deviation plotted as the error bars. **c** Comparison of five-fold average MAE results on MatBench datasets between CLOUD trained from scratch (non-pretrained) and pre-trained with MLM. The MAE results are shown in base-10 logarithm. The percentage reduction in MAE is annotated above each dataset and the error bars are plotted. **d** Receiver operating characteristic (ROC) curves for models evaluated on MatBench Discovery for structure stability classification. False positive rate (FPR) and true positive rate (TPR) are the fraction of nonstable/stable structures classified as stable. Area under curve (AUC) scores are calculated and presented in descending order. **e** Fine-tuning results on UnconvBench general predictive tasks. All results are shown in the mean of test MAE/MAD in five-fold cross-validation along with the standard deviation plotted as the error bars.

the thermodynamic stability of materials. The dataset aims to reflect practical challenges in the discovery process by requiring predictions based on unrelaxed crystal structures, which avoid reliance on expensive DFT calculations. We fine-tune CLOUD on Materials Project [67] formation energy training data and test on WBM dataset [68]

which contains $\sim 257\text{K}$ OOD crystal structures generated by systematically substituting elements in pre-existing structures from Materials Project. Model performance is evaluated in terms of the ROC-AUC score, which is calculated by varying the stability threshold, recording the false positive rate (FPR, the fraction of unstable structures being misclassified as stable) and true positive rate (TPR, the fraction of stable structures that are correctly identified), plotting the ROC (Receiver operating characteristic) curve, and calculating the area under curve (AUC) score. In contrast to directly predicting the formation energy for relaxed structures where CLOUD gives a larger prediction error than many structure-based GNNs, CLOUD manifests comparable classification performance despite not using atomic coordinates, given that the model achieves the AUC score of 0.81 which is close to that of ALIGNN [21] and higher than that of CGCNN [19] and MEGNet [69], as shown in Figure 2d. These results highlight CLOUD’s potential for accelerating materials discovery by effectively screening unrelaxed structures and directly predicting the stability of the relaxed ones, thereby minimizing reliance on costly DFT calculations.

Noticeably, the crystal structures from MatBench or Matbench Discovery datasets are ‘regular’ crystals that predominantly feature well-ordered structures and lack the structural diversity, dimensional variation, or disorder commonly seen in more complex or ‘unconventional’ materials which are, in fact, ‘conventional’ in real-world under finite temperatures. Therefore, we fine-tune the model on crystal structures from UnconvBench [70], which includes crystals with defects, large unit cells, or low-dimensional structures. Different from the cases for MatBench in which the sophisticated structure-based GNN models like coGN [22], coNGN [22], and ALIGNN [21] show superior accuracy, CLOUD demonstrates comparable performance to the SOTA model CrysToGraph [70] and significantly outperforms the other structure-based models (Figure 2e). Such evidence reveals the promising potential of CLOUD to be applied for material discovery. In addition, the best model for each UnconvBench task is either CrysToGraph or CLOUD, both of which take into account global information about crystal structures. Distinct from CrysToGraph which learns the long-range interactions with a graph-wise transformer, CLOUD directly encodes symmetry information via generator strings and Wyckoff positions, providing an alternative for encoding global information for crystal structures. We provide the MAE results for each model on the six predictive tasks in Table S6.

To further understand how the SCOPE representation contributes to better modeling of crystal structures, we examine the attention scores between the [CLS] token and the other tokens. Attention scores indicate the correlation between tokens, thereby reflecting the model’s interpretation of the encoded features. We focus on the attention scores between [CLS] and the other remaining tokens in the sequence because the [CLS] embedding is fed to the prediction head for property prediction and high attention scores likely imply a significant contribution of the corresponding tokens to the material property prediction.

To illustrate, we compute attention scores across hidden layers and attention heads for crystal structures in the *gvrh* test set from MatBench. The attention scores between [CLS] and other tokens are aggregated across attention heads, from which we identify the top- k important tokens with the highest attention scores for each data point. We

prioritize analyzing the attention scores from the first hidden layer as it is closest to the input and consequently learns more semantic information from the sequences [71]. To quantify the relationship between [CLS] and space group tokens, we introduce two probabilities: p_1 , the probability that at least one space group token appears in the top- k list for a given sequence, and p_2 , the proportion of space group tokens among the top- k tokens. We vary k and find that the probability of retrieving at least one space group token among the top- k tokens (p_1) increases from 0.93 at $k = 1$ to 0.99 at $k = 3$, while the average proportion of space group tokens among the top- k tokens (p_2) remains consistently high, ranging from 0.91 to 0.93. This confirms that space group tokens receive significant “attention” (contributions to the machine-learned feature) considering their average portion in a sequence in this dataset is ~ 0.64 . To assess the statistical significance of this prioritization, we perform a one-sample t-test comparing the observed values of p_1 and p_2 to a baseline of 0.5, which serves as the null hypothesis representing random or uniform attention. The test rejects the null hypothesis ($p < 0.001$), indicating that p_1 and p_2 are significantly greater than the expected 0.5. The 95% confidence intervals for p_1 ($[0.9236, 0.9444]$ for $k = 1$, $[0.9820, 0.9916]$ for $k = 2$, $[0.9886, 0.9960]$ for $k = 3$) and p_2 ($[0.9236, 0.9444]$, $[0.9165, 0.9329]$, $[0.9002, 0.9156]$) consistently exceed 0.64, demonstrating that space group tokens are systematically prioritized. These results validate that the model effectively learns symmetry-consistent representations rather than distributing attention based solely on token frequency.

In addition to the evaluation of model prediction accuracy, it is crucial to understand how performance improves with increased model and data—an essential consideration for foundation models as they are often deployed at large scales to achieve generalization and transferability across tasks. Therefore, we further examine how the model performance scales with the number of pre-training data and model parameters. The model performance (cross-entropy loss for the pre-training task) empirically scales with the number of tokens D and non-embedding model parameters N (excluding the model parameters for vectorizing tokens) in a power law relationship, which is expressed by Hoffmann’s scaling law [38]:

$$L(N, D) = \frac{A}{N^\alpha} + \frac{B}{D^\beta} + E \quad (4)$$

We vary the number of pre-training data and non-embedding parameters in the encoder of the model to fit the scaling law accordingly. We solve the optimization problem with the L-BFGS algorithm [72] to obtain the following result:

$$A = 90.7464, B = 21.9854, E = 0.2296, \alpha = 0.4339, \beta = 0.3518$$

With the fitted scaling law, we estimate the optimal model size for a given compute budget. Following the derivation in literature [38], the optimal model size and data size can be written as:

$$N_{opt}(C) = G \left(\frac{C}{6} \right)^a, D_{opt}(C) = G^{-1} \left(\frac{C}{6} \right)^b \quad (5)$$

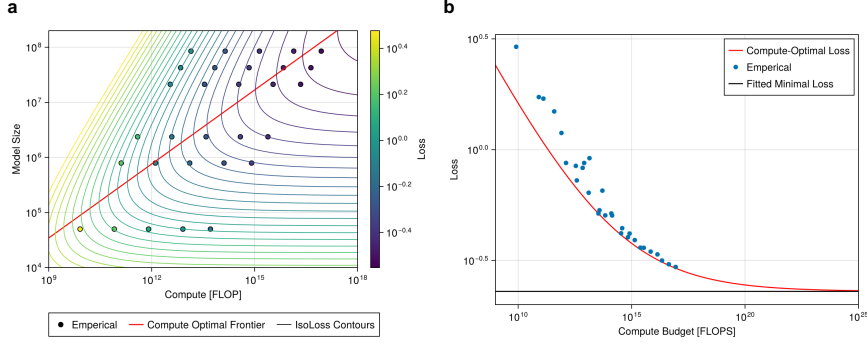


Fig. 3 Training compute optimal models for pre-training CLOUD. **a** Visualization of the scaling law fitted to empirical pre-training loss data. The black dots represent empirical observations, the red line indicates the compute-optimal frontier, and the contour lines represent iso-loss curves derived from the fitted scaling function. **b** Pre-training loss as a function of total compute budget (FLOPs). The blue dots correspond to empirical results, while the red curve shows the compute-optimal loss predicted by the scaling law.

where

$$G = \left(\frac{\alpha A}{\beta B} \right)^{\frac{1}{\alpha + \beta}}, \quad a = \frac{\beta}{\alpha + \beta}, \quad b = \frac{\alpha}{\alpha + \beta} \quad (6)$$

Given the α and β we fitted, we can readily derive that $a = 0.45$ and $b = 0.55$ for CLOUD. Interestingly, the a and b from the empirical scaling law that we fit for CLOUD are close to the values in Hoffmann’s scaling law where $a = 0.46$ and $b = 0.54$ (derived from parametric modeling of the loss) [38]. Given $a \approx b$, the number of parameters and number of tokens should be scaled evenly, unlike the case for Kaplan’s scaling law which infers that the model size should scale faster than the number of tokens ($a = 0.73$, $b = 0.27$) [37].

The fitted scaling law is also visualized in Figure 3. The fitted entropy term E , which reflects the natural entropy of text data, is equal to 0.2296 for CLOUD, significantly lower than the $E = 1.69$ reported in [38], suggesting that the underlying data distribution for CLOUD is more structured or predictable, allowing for a smaller irreducible loss floor. The result aligns with our expectation, as the string representation that we design follows certain rules distilled from chemical knowledge.

Despite the strong scaling performance, the visualization in Figure 3b, however, also reveals the limitation of scaling. The entropy term E , which reflects the natural entropy of the text data, the benefits of scaling diminish because the loss asymptotically approaches E as the compute budget increases, highlighting that beyond a certain compute threshold, additional resources yield diminishing returns. This suggests that while scaling remains beneficial, achieving further gains may require innovations in architecture, optimization, or data efficiency rather than simply increasing model size and training tokens. Specifically, our symmetry-consistent string representation mainly focuses on efficient encoding while not ensuring completeness since this version does not encode free variables in Wyckoff positions and lattice parameters for unit cells. Relevant discussions are also provided in section S1 in Supplementary Information.

Therefore, future work that includes richer information while maintaining efficiency is required for the design of foundation models for crystal structures.

CLOUD-DEBYE: Integration of CLOUD in a differentiable and physics-consistent materials thermodynamics framework

To advance beyond accurate but purely data-driven predictions, we propose integrating CLOUD with physical models to form a differentiable, physics-consistent framework. This enables the model not only to make predictions aligned with known physical laws but also to propagate gradients through those laws, allowing end-to-end training.

As a representative case study, we demonstrate this approach by combining CLOUD with the Debye model to predict temperature-dependent phonon properties such as phonon internal energy (U) and heat capacity (C_v). They arise from collective lattice vibrations that are governed by the global periodicity of the crystal and the vibrational modes spanning multiple unit cells. According to the Debye model [54], U and C_v can be expressed as:

$$U \approx \frac{9}{8}Nk_B\Theta + 9Nk_BT \left(\frac{T}{\Theta}\right)^3 \int_0^{x_D} \frac{x^3}{e^x - 1} dx \quad (7)$$

$$C_v = \left(\frac{\partial U}{\partial T}\right)_V \approx 9Nk_B \left(\frac{T}{\Theta}\right)^3 \int_0^{x_D} \frac{x^4 e^x}{(e^x - 1)^2} dx \quad (8)$$

$$x_D = \frac{\Theta}{T} \quad (9)$$

$$\Theta = \frac{\hbar\omega_D}{k_B} \quad (10)$$

where ω_D is the Debye frequency, N is the number of atoms, \hbar is the reduced Planck constant, k_B is the Boltzmann constant, and T is the temperature. The Debye frequency could be further written as $\omega_D = \left(\frac{6\pi^2 N}{V}\right)^{\frac{1}{3}} v$ where V is the volume of the N atoms and v is the speed of sound in the material. The sound velocity v can be approximated using the first-order Hooke's law as:

$$v \approx \sqrt{\frac{C}{m}} d \quad (11)$$

Here, C denotes the effective spring constant, m is the atomic mass within the primitive cell, and d is the effective interplanar spacing along the direction of vibration. Therefore, U and C_v depend on lattice volume, bonding strength, and sound velocity — all of which are inherently long-range characteristics of the crystal structure. As a result, accurate prediction of U and C_v requires models capable of capturing these long-range structural dependencies and periodic constraints. However, recent systematic analyzes have shown that convolution-based Graph Neural Networks (GNNs) face inherent limitations in this regard [27, 73]. Specifically, GNNs are prone to over-smoothing [74, 75] and over-squashing [76, 77], which restrict their receptive fields and

impair their ability to learn long-range dependencies across the crystal. As a result, they often struggle with modeling properties that are sensitive to global structure. Transformer-based language models offer a promising alternative. Unlike GNNs, they capture interactions between all tokens without relying on sequential message passing, thereby enabling the modeling of long-range dependencies. Our proposed model, CLOUD, is built upon such a language model architecture and leverages the SCOPE representation, which directly encodes the space group—a global symmetry descriptor of the crystal. This makes CLOUD particularly well-suited for capturing the periodic and long-range features required for phonon property prediction. To evaluate this capability, we first evaluate CLOUD on the internal energy (U) and heat capacity (C_v) datasets curated by Gong et al [27]. These datasets, constructed from Materials Project entries [67], include DFT-computed phonon properties derived from phonon density of states (DOS) at 300K. By comparing performance on these tasks, we aim to assess whether language models can surpass state-of-the-art GNNs in learning the global structural representations necessary for accurate phonon property prediction.

Meanwhile, the original benchmarking experiments in the literature [27] are conducted by predicting the U and C_v values at $T = 300K$ directly from the models. Such an experimental setting comes with an obvious limitation that the model cannot learn the temperature dependency of C_v and U . In other words, learning the mapping between crystal structures and those properties is intrinsically ill-posed. Possible solutions include training different models for different temperatures or encoding temperature explicitly in the crystal embeddings, but both of them are computationally expensive as C_v labels under different temperatures are required, and they do not satisfy the thermodynamic consistency. According to Debye model, the phonon internal energy and heat capacity per unit cell is given by Equation 7 and 8, respectively [54]. Contrary to C_v and U , the Debye temperature Θ is not dependent on the temperature but rather an intrinsic property of crystal structures. Gong et al. [27] claimed that the concatenation of descriptors improves the modeling of Θ , whereas the thermodynamic consistency is still not achieved. Therefore, we propose CLOUD-DEBYE which is an integration of CLOUD and Debye model – CLOUD predicts Θ which is fed to Debye model for predicting C_v and U . The differentiable implementation of Debye model enables training with C_v or U labels end-to-end without requiring the knowledge of Debye temperature.

The evaluation results for predicting U and C_v are presented in Table 1. The model performance is evaluated according to the metric MAE/MAD. Usually, a model will be considered as a good predictive model if $MAE/MAD < 0.2$ [21, 78]. While all the GNNs result in high MAE/MAD values, CLOUD, without the integration of Debye model, reaches 0.16 and 0.15 on C_v and U , respectively. CLOUD-DEBYE further reduces the MAE/MAD metric significantly, outperforming all the descriptor-hybridized GNNs proposed by Gong et al. [27] which aimed to compensate the lack of long-range information by concatenating global descriptors. The results manifest CLOUD’s capability of learning long-range dependencies in crystal structures as well as the significance of introducing thermodynamic consistency into the material machine learning framework. Interestingly, CLOUD-DEBYE achieves improved prediction accuracy than the purely data-driven CLOUD model pre-trained on $\sim 6.3M$

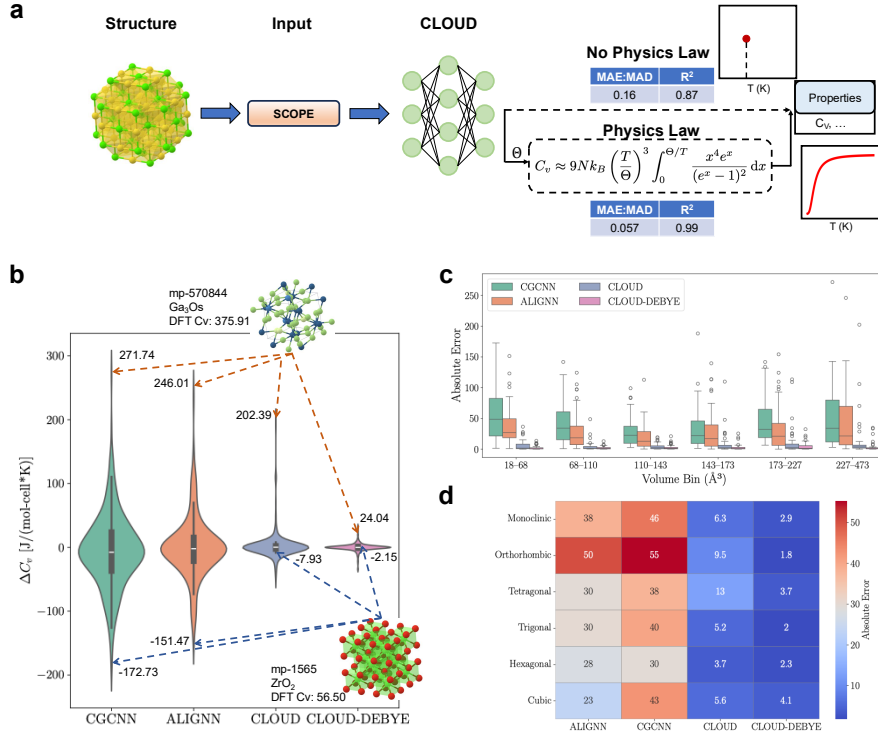


Fig. 4 CLOUD-DEBYE, a differentiable-physics framework with CLOUD. **a** Integration of physics laws with CLOUD model. The example exhibits the prediction for constant-volume heat capacity (C_v) where CLOUD outputs the Debye temperature (Θ) and the Debye model predicts C_v using Θ as input under different temperatures. **b** The violin plot of the prediction errors in C_v by CGCNN, ALIGNN, CLOUD, and CLOUD-DEBYE. Two example structures from the C_v test set are shown: mp-570844 (Ga_3O_5) and mp-1565 (ZrO_2), and the corresponding residual ΔC_v and C_v targets from the test set are marked in the figure. **c** Box plot of absolute errors in C_v prediction across six equal-sized bins sorted by primitive cell volume. Each bin contains approximately the same number of data points to ensure balanced comparison. **d** Heatmap of C_v prediction errors grouped by crystal system. Each cell shows the mean absolute error for a given space group, with crystal systems annotated along the y-axis for symmetry context.

data, even when trained from scratch. This underscores the importance of correctly incorporating physical principles: by enforcing thermodynamic consistency through the Debye model, CLOUD-DEBYE benefits from strong inductive bias that leads to accurate and physically valid predictions. These results highlight that proper integration of physics is as important as, if not more important than, advances in machine learning techniques for building scientific foundation models.

We further visualize the error in C_v prediction ($C_{v,target} - C_{v,predict}$) by different models in Figure 4b. Compared to CGCNN [19] and ALIGNN [21], two competitive GNNs for material property predictions, which exhibit wide distributions and high variability of ΔC_v , the CLOUD and CLOUD-DEBYE error distributions exhibit much smaller spread. Noticeably, CLOUD-DEBYE results in a much narrower error distribution and substantially reduces the maximum absolute error by more than a factor

Table 1 Results on predicting heat capacity (C_v) and phonon internal energy (U). All results are shown in the mean of test MAE/MAD in five-fold cross-validation along with the standard deviation in brackets. The best results are in bold and the second-best results are underlined. CLOUD-DEBYE is evaluated for both trained-from-scratch (denoted as CLOUD-DEBYE_{scratch}) and pretrained-then-finetuned (denoted as CLOUD-DEBYE_{FT}). Descriptor-hybridized GNNs are denoted as de-GNN.

Model	C_v (\downarrow)	U (\downarrow)
CGCNN	0.76 (0.03)	0.71 (0.03)
ALIGNN	0.63 (0.03)	0.53 (0.03)
MEGNet	0.71 (0.03)	0.64 (0.02)
Matformer	0.44 (0.02)	0.46 (0.02)
de-CGCNN	<u>0.058 (0.004)</u>	0.060 (0.005)
de-ALIGNN	0.089 (0.006)	0.10 (0.01)
de-MEGNet	0.058 (0.005)	<u>0.057 (0.005)</u>
de-Matformer	0.13 (0.01)	<u>0.14 (0.01)</u>
CLOUD	0.16 (0.00)	0.15 (0.00)
CLOUD-DEBYE _{scratch}	0.091 (0.002)	0.11 (0.01)
CLOUD-DEBYE _{FT}	0.057 (0.001)	0.055 (0.003)

of six, suggesting that integration with Debye model leads to more consistent C_v predictions. Two representative structures, Ga_3Os (mp-570844) and ZrO_2 (mp-1565), are highlighted to illustrate this effect: while CGCNN and ALIGNN exhibit errors exceeding 150–270 J/(mol-cell*K), CLOUD-DEBYE produces much more accurate predictions, reducing the error to 6.5% of the target value from the dataset, or even lower. Furthermore, CLOUD-only fails to lower the error and still results in unphysical predictions without the integration of the Debye model. Such a result indicates that even when using the same model architecture and training objective, physics integration constrains unphysical outliers and enforces more reliable predictions. Figure 4c and d further examine the error distribution with respect to structural characteristics. In Figure 4c, the test set data are grouped by primitive cell volume, revealing that CGCNN [19] and ALIGNN [21] struggle particularly with large-volume structures, often producing substantial or unphysical errors. This trend reflects the limitations of GNNs with finite receptive fields, which hinder their ability to capture long-range interactions essential for accurate C_v prediction in extended systems, consistent with the observation by Gong et al. [27]. In contrast, CLOUD significantly reduces the error across all volume bins, and CLOUD-DEBYE further improves upon this, achieving low and stable errors even for the largest structures. Figure 4d presents a heatmap of average error across crystal systems, where CLOUD-DEBYE consistently outperforms all GNNs and purely data-driven CLOUD. The error reduction is especially notable for complex systems such as orthorhombic, tetragonal, trigonal, and hexagonal crystals, underscoring the generalizability of physics-informed modeling across diverse symmetry classes. Therefore, the results highlight CLOUD’s superior accuracy and robustness

for learning features relevant to C_v prediction, and also demonstrate the potential of combining it with physics-based models for real-world material applications.

After being trained on C_v data at $T = 300\text{K}$, CLOUD-DEBYE can be extrapolated to predict C_v at other temperatures. We evaluate the model performance on different chemical systems: Al_2O_3 and Li_2O are two oxides, $CaTiO_3$ belongs to perovskite, and GaN is a III-V compound which is broadly used as semiconductors. We vary the temperature from 0 K to near the melting points of the compounds. The predictions are compared to experimental results reported in previous literature [79–82] as well as phonon calculation results with Perdew-Burke-Ernzerhof (PBE) as the exchange-correlation functional from the Materials Data Repository (MDR) database [83]. As experiments are usually conducted under constant pressure, the experimental results are reported as constant-pressure heat capacity (C_p) which differs from C_v by $C_p - C_v = \frac{\alpha^2 TV}{\kappa_T}$ where α is the expansion coefficient and κ_T is the isothermal compressibility. However, C_p is usually a good approximation for C_v of solids under low temperature [54].

The prediction results by CLOUD-DEBYE are visualized in Figure 5. For all the four systems that are experimented with, the CLOUD-DEBYE’s prediction results match the experimental and DFT-calculated values well under different temperatures, even though the model is only trained with C_v under 300K. In addition, $CaTiO_3$ is not included in either of the training or test set, which reflects the superior generalization performance of our model. Furthermore, the integration of Debye model ensures the thermodynamic consistency of model predictions. According to Debye model, the heat capacity approaches

$$C_v \rightarrow 9Nk_B \left(\frac{T}{\Theta}\right)^3 \int_0^{x_D} x^2 dx = 3Nk_B \quad (12)$$

as $T \rightarrow \infty$, which is expected (Dulong-Petit Law), since at high temperatures all phonon modes become activated. In the limit of $T \rightarrow 0$,

$$C_v \rightarrow 9Nk_B \left(\frac{T}{\Theta}\right)^3 \int_0^\infty \frac{x^4 e^x}{(e^x - 1)^2} dx \sim Nk_B \frac{T^3}{\Theta^3} \quad (13)$$

Both of the two constraints are satisfied by the model predictions.

The results above strongly suggest the advantage of combining deep learning model with physics-based model as the temperature dependence of C_v is directly embedded in the model, improving the data efficiency along the temperature dimension. Previous literature [11] has discussed the challenges of developing empirical [84, 85] or machine-learning models for temperature-dependent heat capacity, primarily due to the difficulty of obtaining thermochemical property data as a function of temperature. Gurunathan et al.[48] alleviated this problem with a DOS-mediated approach: the ALIGNN force field [21] is trained to predict phonon Density of States (pDOS) from which the phonon-based properties including C_v could be derived. In contrast, our model integrates Debye model into the learning framework so that it can be trained end-to-end with C_v data, learning the features to predict Θ from the crystal structures while not requiring any DFT-calculated labels of pDOS or Θ . We expect the model

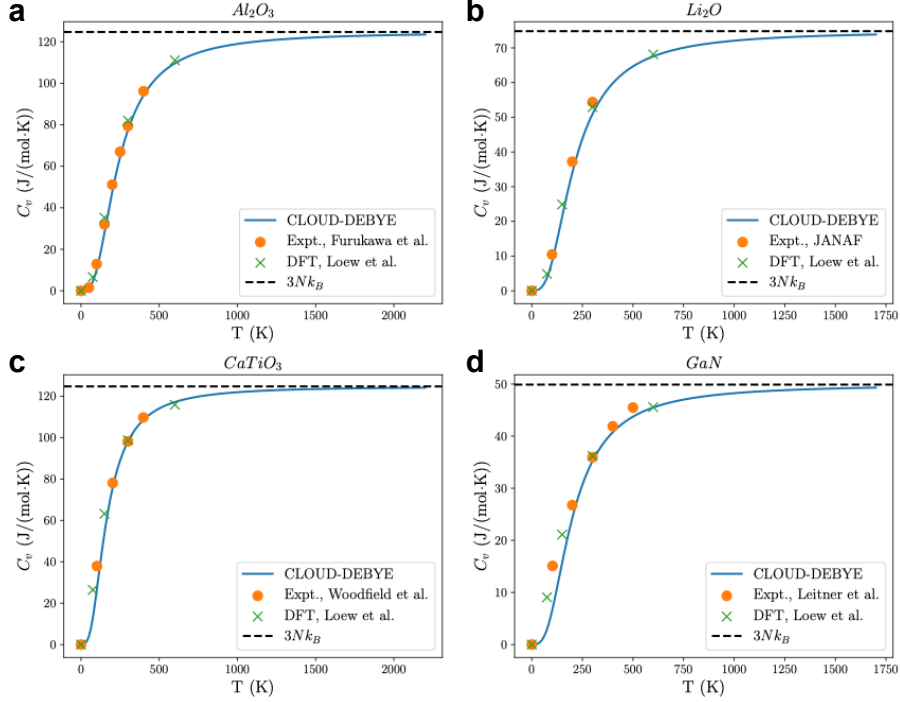


Fig. 5 C_v predictions by CLOUD-DEBYE for **a** Al_2O_3 , **b** Li_2O , **c** $CaTiO_3$, and **d** GaN . The CLOUD-DEBYE model, fine-tuned on C_v data at 300K, accurately extrapolates heat capacity across a wide temperature range, approaching the melting point of each material. Model predictions are compared against experimental and DFT-calculated results. The Dulong-Petit limit ($3Nk_B$) is included as a reference.

to serve as a differentiable framework that learns essential physical properties of crystal structures from data of high-quality and easy-accessibility and predicts material properties while observing physics consistency.

Discussion

In this work, we introduce CLOUD, a scalable and physics-informed foundation model for crystal representation learning that combines symmetry-consistent representations with large-scale pretraining and finetuning. CLOUD leverages a novel symmetry-consistent string representation, SCOPE, to encode space group symmetries, Wyckoff positions, and elemental compositions in a compact and coordinate-free format. Pre-trained on over six million unlabeled crystal structures and fine-tuned on labeled data of diverse downstream tasks, CLOUD achieves competitive performance across a wide range of material property prediction tasks, while exhibiting strong generalization in data-limited and out-of-distribution scenarios.

Our findings reveal several key takeaways. Firstly, the explicit encoding of symmetry significantly improves the predictive accuracy over previous coordinate-free approaches or even GNNs that directly encoding 3D atomic coordinates. SCOPE

forms a hierarchical representation consisting of global symmetries to equivalent sites and material compositions, thus accomplishing an efficient representation of crystal structures. The strong attention scores toward space group tokens in the SCOPE representation further confirm the model’s capability to prioritize physically meaningful structural descriptors. The results highlight the significance of integrating symmetry constraints directly into the material representations, which receives little attention in most of prior models that treat crystal structures as generic graphs or sequences.

In addition, we demonstrate that scaling laws observed in natural language processing models also apply to the foundation model for crystals. CLOUD manifests strong scaling behavior with respect to both model size and dataset size, closely aligning with the predictions of Hoffmann’s scaling framework. This insight opens up new opportunities for building larger, more powerful crystal foundation models that scale predictably with resources.

Moreover, CLOUD is capable of learning long-range structural dependencies. Traditional GNN-based methods often suffer from limited receptive fields due to over-smoothing and over-squashing. In contrast, the transformer architecture of CLOUD, combined with symmetry-consistent representations, enables superior performance on tasks that depend on global structural features, such as predicting heat capacity and internal energy. This is particularly evident in the integration with the Debye model, where CLOUD-DEBYE not only achieves better predictive performance but also ensures thermodynamic consistency across wide temperature ranges.

The integration of physics laws into differentiable frameworks offers a compelling direction for scientific machine learning, enabling models to produce predictions that are not only accurate but also physically consistent. By embedding analytical expressions, such as the Debye model, within the learning pipeline, CLOUD learns to predict physically meaningful intermediate quantities like the Debye temperature and propagates gradients through the physical laws to enforce thermodynamic constraints. This end-to-end differentiable setup contrasts with prior approaches that either predict target properties directly or rely on post hoc corrections. Our results highlight that incorporating physics laws into foundation models is not merely an enhancement but a critical design principle for achieving robust, generalizable, and scientifically solid predictions.

Several promising directions remain for future exploration. Despite CLOUD’s strong scaling performance with respect to data size, the availability of high-quality crystal data for pretraining remains limited. Therefore, constructing a large-scale, high-quality crystal structure database would be instrumental in advancing scientific foundation models for crystals. Moreover, the current design of SCOPE can be further refined. Currently, SCOPE represents an ensemble of crystal structures that share the same space group, Wyckoff positions, and composition but differ in atomic coordinates due to the presence of free parameters in many Wyckoff positions.

In a nutshell, CLOUD serves as a unified foundation model that bridges machine learning and domain physics, providing a scalable and physically consistent framework for crystal property prediction. Its success in generalization, efficiency, and integration with physics laws makes it a promising tool for accelerating discovery in materials science and beyond.

Methods

Symmetry-Consistent Ordered Parameter Encoding

We design Symmetry-Consistent Ordered Parameter Encoding (SCOPE), a symmetry-consistent string representation for crystal structures that integrates symmetry, equivalent sites, and constituting atoms to efficiently encode the structural and compositional information, eliminating the need for coordinate information or equivariant models. A SCOPE string for a crystal structure starts with the generator string which represents the basic symmetry operators of the corresponding space group. To build the generator string for each space group, all non-translational symmetry operations are represented by 14 generator matrices labeled a to n , while 10 uppercase letters encode translation components. Together, these generators define all symmetry operators and enable encoding all 230 space groups in a compact 4104-byte ASCII file [60].

Take the No. 35 space group as an example. Its generator string is given by ‘03aDDDbOOOjOOO0’. The ‘0’ at the beginning of the generator string indicates the inversion operator is not a generator. After that, ‘3’ indicates that there are three generator matrices. Every four letters correspond to a generator: the first lower-case letter determines which of the 14 matrices is to be used, and the subsequent 3 letters stand for the translation components in three dimensions. For instance, ‘aDDO’ corresponds to the symmetry operator:

$$g = \begin{pmatrix} \mathbf{O} & \mathbf{t} \\ \mathbf{0} & 1 \end{pmatrix} = \begin{pmatrix} 1 & 0 & 0 & \frac{1}{2} \\ 0 & 1 & 0 & \frac{1}{2} \\ 0 & 0 & 1 & 0 \\ 0 & 0 & 0 & 1 \end{pmatrix} \quad (14)$$

The last symbol in the generator string is ‘0’ which indicates that there is not any alternative choice of the origin for this space group.

We argue that generator strings are more informative than space group symbols, as space group symbols only provide a high-level classification of symmetry, whereas generator strings offer detailed insight into the specific symmetry operations that define the crystal’s structure. For example, $Cmc2_1$ (No. 36) and $Amm2$ (No. 38) only have one character in common in the space group symbols. However, their generator strings are ‘03aDDObOODjOOD0’ and ‘03aODDbOOOjOOO0’, respectively, suggesting that their symmetry generators are quite similar and only differ in the translation components. In fact, both space groups belong to the orthorhombic crystal system and exhibit mirror planes and two-fold rotation axes, but the subtle difference in the translation components (specifically in glide operations) reflects the underlying structural variation. This distinction is not apparent from the space group symbols alone, highlighting the value of generator strings in capturing more nuanced symmetry information. In contrast, $Fmm2$ (No. 42) has a face-centered lattice while $Imm2$ (No. 44) has a body-centered lattice, and the difference in lattice type significantly affects the symmetry operations and translations within the unit cell even though they both belong to Orthorhombic crystal system. Their space group names have 75% of the characters in common. Instead, their generator strings, ‘04aODDaDODbOOOjOOO0’

and ‘03aDDDbOOOjOOO0’, reflect more difference in the symmetry operators than their names.

Wyckoff positions in a SCOPE string are denoted by a symbol containing a number and a letter, e.g., $4d$. The number denotes how many elements are on the corresponding orbit, also known as the “multiplicity” of the site. The letter is used to distinguish the different Wyckoff positions for a specific space group. The assignment rule for letters is the letters showing up earlier in the alphabet are given to sites with lower multiplicity.

Finally, the generator string for the space group, the Wyckoff symbols for atomic positions, and material compositions (e.g. $NaCl$, Al_2O_3 , $CaTiO_3$, etc.) are integrated to form a coordinate-free representation of crystals while maintaining crucial structural information like symmetries, enabling efficient encoding of crystal structures so that large language models can be utilized for crystal representation learning. To construct the SCOPE representation, we parse CIF files using pymatgen [86] to extract structural and symmetry information. For each structure, we apply ‘SpacegroupAnalyzer’ to determine its space group number and Wyckoff positions, and consequently retrieve the generator strings corresponding to the space groups. Finally, the material composition is extracted from the structure’s fractional composition and appended to form the complete string. This results in a sequence of the form: [generator string] | [Wyckoff symbols] | [composition], efficiently capturing structural symmetry and stoichiometry without relying on atomic coordinates.

Datasets

Pre-train Dataset. For CLOUD pre-training, we collect ~ 6.3 M unique crystal structures from Open Databases Integration for Materials Design (OPTIMADE) [53] API. OPTIMADE integrates data from various major materials databases and provides an application programming interface (API) to make the data accessible to users. The contributing databases include: AFLOW [87], Alexandria [88], Computational Two-Dimensional Materials Database (C2DB) [89], Crystallography Open Database (COD) [90], Joint Automated Repository for Various Integrated Simulations (JARVIS) [91], Materials Cloud [92], Materials Platform for Data Science (MPDS) [93], Materials Project [67], Material-Property-Descriptor Database (MPDD) [94], Material Properties Open Database (MPOD) [95], NOMAD [96], Open Database of Xtals (odbx) [97], Open Materials Database (omdb) [98], and Open Quantum Materials Database (OQMD) [99]. Therefore, such comprehensive datasets enable effective pre-training on crystal representations. The original data we downloaded from OPTIMADE consists of ~ 13 M CIF files. We de-duplicate the data by only keeping the structure with the smallest volume per volume when several CIF files have exactly the same chemical formula and space group. Finally, we use the de-duplicated ~ 6.3 M data as the pre-training set.

Fine-tune Datasets. We evaluate CLOUD across a range of materials datasets that test different aspects of model performance. These include:

- **MatBench** [65], a diverse suite of materials property prediction tasks based on DFT and experimental data. We focus on eight regression tasks that include structural

Table 2 Summary of the 8 regression tasks from MatBench, MatBench Discovery datasets, the 6 general predictive tasks from UnconvBench, and two phonon-related datasets C_v and U from Gong et al. [27] used in this paper.

Dataset	Task	Size	Property	Unit
MatBench	jdft2d	636	Exfoliation energy of 2D materials	meV/atom
	phonons	1265	Highest phonon peak frequency	cm^{-1}
	dielectric	4764	Refractive index	unitless
	gvrh	10987	Log10 of VRH average shear moduli	log GPa
	kvrh	10987	Log10 of VRH average bulk moduli	log GPa
	perovskites	18928	Formation energy of perovskites	eV/unit cell
	band gap	106113	Band gap	eV
	e form	132752	Formation energy	eV/atom
MB Discovery	MP (train)	154718	Formation energy	ev/atom
	WBM (test)	256963	Formation energy	ev/atom
UnconvBench	2d_e_exf	4527	Exfoliation energy of 2D materials	eV/atom
	2d_e_tot	3520	Total energy of 2D crystals	eV
	2d_gap	3520	Band gap of 2D materials	eV
	qmof	5106	Formation energy of MOFs	eV
	supercon	1058	Curie temperature	K
	defected	530	Formation energy of defects	eV/atom
Phonon [27]	C_v	1512	Constant-volume heat capacity	J/(mol-cell*K)
	U	1512	Phonon internal energy	kJ/mol-cell)

information and are widely used to assess model accuracy across various physical and chemical properties.

- **MatBench Discovery** [66], which focuses on predicting the stability of novel materials using models trained on customized formation energy data. The evaluation set comprises approximately 257,000 out-of-distribution crystal structures generated through elemental substitution [68]. Summary results are provided in the main text, with detailed evaluation in the Supplementary Information.
- **UnconvBench** [70], a dataset of unconventional crystal systems, including low-dimensional materials, metal-organic frameworks (MOFs), and defected structures. It provides a challenging testbed for assessing model robustness beyond well-ordered bulk crystals. Key results are summarized in the main text, with full analysis in the Supplementary Information.
- **Phonon thermodynamics dataset** [27], which includes phonon internal energy (U) and constant-volume heat capacity (C_v) computed at 300K for Materials Project structures [67]. These properties are derived from phonon density of states (DOS) and reflect long-range structural periodicity and bonding strength. We use this dataset to examine CLOUD’s ability to capture global structural features relevant for thermodynamic property prediction.

We include the information about the fine-tuning datasets that are used in this work in Table 2. More information about the fine-tuning datasets can be found in section S2.1 in Supplementary Information.

Training Details

The CLOUD model is developed upon the transformer encoder architecture [33, 34]. Specifically, it employs Scaled Dot-Product Attention, which computes attention scores by measuring query-key alignment, scaling by the dimension of key, and applying softmax to derive weighted values:

$$\text{Attention}(Q, K, V) = \text{Softmax}\left(\frac{QK^T}{\sqrt{d_k}}\right)V \quad (15)$$

Multi-head attention extends single attention by applying multiple linear projections to Q, K, and V, enabling parallel attention computations. The resulting outputs are concatenated and re-projected to form the final representation, allowing the model to capture diverse subspace information effectively.

CLOUD is first pre-trained via Masked Language Modeling (MLM) on the dataset collected from OPTIMADE. The model is pre-trained in a self-supervised learning approach: without requiring the explicit supervision of labeled data, the model leverages intrinsic structure or patterns within the input data for learning. During pre-training, 15% of the tokens in a sequence are selected for potential modification, among which 80% are masked, 10% are replaced with randomly chosen vocabulary tokens, and the remaining 10% are left unchanged. The strategy, which is consistent with the original implementation proposed in literature[34], ensures the model learns meaningful contextual embeddings while biasing representations toward the actual observed tokens. The pre-training dataset is split into training and validation set by 80/20. AdamW optimizer is used with a learning rate of 5×10^{-5} along with a cosine learning decay. The model is trained with batch size 2048 for a total of 50 epochs.

For the downstream task fine-tuning, we add a randomly initialized MLP after the encoder to output the property predictions. For MatBench, UnconvBench, and U and C_v datasets, five-fold cross-validation is performed and the model is evaluated according to the average score on the test set; for MatBench Discovery, the Materials Project data are split into the training and validation set by 95/5 and the model is evaluated according to the performance on the WBM test set. We perform hyperparameter tuning for each dataset separately for optimal model performance. We provide additional information on model implementation in section S2.2 in Supplementary Information. To ensure a fair comparison on datasets from MatBench, we limit the prediction head for the three pre-trained language models (MatInFormer [30], SLICES-BERT where we train on SLICES [29] with the same architecture as CLOUD, and our CLOUD in this work) to be a single-layer MLP to ensure consistency with MatInFormer architecture implementation [30]. All the baseline results except for SLICES-BERT are obtained from the MatBench leaderboards [65]. When fine-tuned on MatBench Discovery for crystal structure stability classification, the model is first trained to predict the formation energy of the given structure. Based on the predictions for formation energies, the energy above the convex hull (E_{hull}), the distance to the convex hull spanned by competing phases in the same chemical system, is readily obtained to determine the stability of the materials. A material will be classified as stable if its E_{hull} is lower than a threshold. The stability threshold for E_{hull} , typically set to 0, could be dynamically adjusted in order to account for the systematic prediction shifts unique to each model.

Therefore, we vary the threshold and take an record of the statistics such as true positive rate (TPR) and false positive rate (FPR) which are used for further analysis.

When fine-tuning the model on the phonon internal energy (U) and constant-volume heat capacity (C_v) datasets with the CLOUD-DEBYE framework, we integrate the pre-trained CLOUD with the Debye model. Specifically, CLOUD is trained to predict the Debye temperature (Θ), a characteristic property of the crystal structure that governs the temperature dependence of $U(T)$ and $C_v(T)$ through the Debye model. This approach introduces an inductive bias grounded in solid-state physics, enabling the model to generalize more effectively across temperatures. Moreover, while experimental or high-fidelity computational labels for C_v are relatively accessible, direct labels for Θ are more difficult to obtain. By leveraging the Debye model as an intermediate physical prior, CLOUD indirectly learns to predict Θ from the structure and derives $U(T)$ and $C_v(T)$ accordingly. To enable end-to-end training with U or C_v as supervision targets, we adopt a differentiable implementation of the Debye model (Equations 7 and 8), where the integrals are evaluated using Gauss-Legendre quadrature in PyTorch to allow gradient backpropagation through the physical model.

Scaling Analysis

Transformer-based language models benefit from the implicit parallelism of the attention mechanism and exhibit predictable performance improvements as a function of scale. Empirical studies have shown that model performance, often measured via cross-entropy loss, follows power-law scaling laws with respect to both the number of model parameters and the amount of training data [37]. A canonical form of the scaling law introduced by Kaplan et al. [37] is:

$$L(N, D) = \left[\left(\frac{N_c}{N} \right)^{\frac{\alpha_N}{\alpha_D}} + \frac{D_c}{D} \right]^{\alpha_D} \quad (16)$$

where N is the number of tokens, D is the number of non-embedding model parameters, and N_c , D_c , α_N , α_D are dataset-dependent empirical constants. This formulation captures the trade-off between model capacity and training data volume under a fixed compute budget.

To better capture the behavior of loss in realistic settings and account for the irreducible entropy of the data distribution, Hoffmann et al. [38] propose a refined scaling law:

$$L(N, D) = \frac{A}{N^\alpha} + \frac{B}{D^\beta} + E \quad (17)$$

where A , B , E , α , and β are fitting parameters. The constant term E reflects the intrinsic entropy of the data distribution and defines the lower bound on achievable loss.

We evaluate the scaling performance of the proposed CLOUD model by systematically varying the number of pretraining tokens and the number of non-embedding parameters in the BERT encoder. We fit the empirical scaling behavior using the Hoffmann scaling law (Equation 17) to capture the interaction between model size and dataset scale.

The fitting process involves solving the following optimization problem:

$$\min_{A,B,E,\alpha,\beta} \sum_i \text{Huber}_\delta \left(\log \hat{L}(N_i, D_i) - \log L_i \right) \quad (18)$$

where $\hat{L}(N_i, D_i)$ is the predicted loss from the scaling law and L_i is the observed loss for the (N_i, D_i) configuration. We use the Huber loss with threshold $\delta = 10^{-3}$, which provides robustness to outliers, as recommended in Hoffmann et al. [38]. The optimization is performed using the L-BFGS algorithm [72], with multiple random initializations to avoid suboptimal local minima.

This analysis allows us to estimate the compute-optimal scaling trajectory for CLOUD. By identifying the exponents α and β , we can characterize how performance scales with additional compute and whether improvements are better obtained by increasing model size or dataset size. Similar to the findings of Hoffmann et al. [38], we observe that balanced scaling of model size and data yields optimal performance under fixed compute constraints, underscoring the importance of data collection alongside model architecture design.

Data Availability

All data used in this work are publicly available. Original datasets could be found in the corresponding literature [27, 53, 65, 66, 70]. The processed datasets used for model training are deposited in Github for public accession for noncommercial, research purposes at <https://github.com/ChangwenXu98/CLOUD>.

Code Availability

The codes developed for this work are available at <https://github.com/ChangwenXu98/CLOUD>.

Acknowledgements

An award for computer time was provided by the U.S. Department of Energy’s (DOE) Innovative and Novel Computational Impact on Theory and Experiment (INCITE) Program. This research used resources from the Argonne Leadership Computing Facility, a U.S. DOE Office of Science user facility at Argonne National Laboratory, which is supported by the Office of Science of the U.S. DOE under Contract No. DE-AC02-06CH11357. This work was supported by Los Alamos National Laboratory under the grant number AWD026741 at the University of Michigan. The author thanks Advanced Research Computing at the University of Michigan for providing computing resources.

Author Contributions

C.X., S.Z., and V.V. designed research; C.X., S.Z., and V.V. contributed to the conceptualization and methodology of the SCOPE representation and CLOUD/CLOUD-DEBYE framework; C.X. implemented the algorithms; C.X., S.Z., and V.V. analyzed

data and wrote the paper; V.V. supervised the work; all authors modified and approved the manuscript.

Competing Interests

The authors declare no competing financial or non-financial interests.

References

- [1] Wang, M., Pan, N.: Predictions of effective physical properties of complex multiphase materials. *Materials Science and Engineering: R: Reports* **63**(1), 1–30 (2008)
- [2] Pilania, G., Wang, C., Jiang, X., Rajasekaran, S., Ramprasad, R.: Accelerating materials property predictions using machine learning. *Scientific reports* **3**(1), 2810 (2013)
- [3] Ahmad, Z., Xie, T., Maheshwari, C., Grossman, J.C., Viswanathan, V.: Machine learning enabled computational screening of inorganic solid electrolytes for suppression of dendrite formation in lithium metal anodes. *ACS central science* **4**(8), 996–1006 (2018)
- [4] Tabor, D.P., Roch, L.M., Saikin, S.K., Kreisbeck, C., Sheberla, D., Montoya, J.H., Dwaraknath, S., Aykol, M., Ortiz, C., Tribukait, H., *et al.*: Accelerating the discovery of materials for clean energy in the era of smart automation. *Nature reviews materials* **3**(5), 5–20 (2018)
- [5] Pyzer-Knapp, E.O., Pitera, J.W., Staar, P.W., Takeda, S., Laino, T., Sanders, D.P., Sexton, J., Smith, J.R., Curioni, A.: Accelerating materials discovery using artificial intelligence, high performance computing and robotics. *npj Computational Materials* **8**(1), 84 (2022)
- [6] Giustino, F.: *Materials Modelling Using Density Functional Theory: Properties and Predictions*. Oxford University Press, Oxford (2014)
- [7] Dave, A., Mitchell, J., Burke, S., Lin, H., Whitacre, J., Viswanathan, V.: Autonomous optimization of non-aqueous li-ion battery electrolytes via robotic experimentation and machine learning coupling. *Nature communications* **13**(1), 5454 (2022)
- [8] Annevelink, E., Kurchin, R., Muckley, E., Kavalsky, L., Hegde, V.I., Sulzer, V., Zhu, S., Pu, J., Farina, D., Johnson, M., Gandhi, D., Dave, A., Lin, H., Edelman, A., Ramsundar, B., Saal, J., Rackauckas, C., Shah, V., Meredig, B., Viswanathan, V.: Automat: Automated materials discovery for electrochemical systems. *MRS Bulletin* **47**(10), 1036–1044 (2022) <https://doi.org/10.1557/s43577-022-00424-0>

- [9] Nørskov, J.K., Bligaard, T., Rossmeisl, J., Christensen, C.H.: Towards the computational design of solid catalysts. *Nature chemistry* **1**(1), 37–46 (2009)
- [10] Grimvall, G.: *Thermophysical Properties of Materials*. Elsevier, Amsterdam (1999)
- [11] Kauwe, S.K., Graser, J., Vazquez, A., Sparks, T.D.: Machine learning prediction of heat capacity for solid inorganics. *Integrating Materials and Manufacturing Innovation* **7**, 43–51 (2018)
- [12] Shankar, R.: *Principles of Quantum Mechanics*. Springer, New York (2012)
- [13] McCullough, K., Williams, T., Mingle, K., Jamshidi, P., Lauterbach, J.: High-throughput experimentation meets artificial intelligence: a new pathway to catalyst discovery. *Physical Chemistry Chemical Physics* **22**(20), 11174–11196 (2020)
- [14] Chen, C., Nguyen, D.T., Lee, S.J., Baker, N.A., Karakoti, A.S., Lauw, L., Owen, C., Mueller, K.T., Bilodeau, B.A., Murugesan, V., *et al.*: Accelerating computational materials discovery with machine learning and cloud high-performance computing: from large-scale screening to experimental validation. *Journal of the American Chemical Society* **146**(29), 20009–20018 (2024)
- [15] Hellenbrandt, M.: The inorganic crystal structure database (icsd)—present and future. *Crystallography Reviews* **10**(1), 17–22 (2004)
- [16] Davies, D.W., Butler, K.T., Jackson, A.J., Morris, A., Frost, J.M., Skelton, J.M., Walsh, A.: Computational screening of all stoichiometric inorganic materials. *Chem* **1**(4), 617–627 (2016)
- [17] Phuthi, M.K., Yao, A.M., Batzner, S., Musaelian, A., Guan, P., Kozinsky, B., Cubuk, E.D., Viswanathan, V.: Accurate surface and finite-temperature bulk properties of lithium metal at large scales using machine learning interaction potentials. *ACS Omega* (2024)
- [18] Gilmer, J., Schoenholz, S.S., Riley, P.F., Vinyals, O., Dahl, G.E.: Neural message passing for quantum chemistry. In: *International Conference on Machine Learning*, pp. 1263–1272 (2017). PMLR
- [19] Xie, T., Grossman, J.C.: Crystal graph convolutional neural networks for an accurate and interpretable prediction of material properties. *Physical review letters* **120**(14), 145301 (2018)
- [20] Goodall, R.E., Lee, A.A.: Predicting materials properties without crystal structure: Deep representation learning from stoichiometry. *Nature communications* **11**(1), 6280 (2020)

- [21] Choudhary, K., DeCost, B.: Atomistic line graph neural network for improved materials property predictions. *npj Computational Materials* **7**(1), 185 (2021)
- [22] Ruff, R., Reiser, P., Stühmer, J., Friederich, P.: Connectivity optimized nested graph networks for crystal structures. *arXiv preprint arXiv:2302.14102* (2023)
- [23] Ihalage, A., Hao, Y.: Formula graph self-attention network for representation-domain independent materials discovery. *Advanced Science* **9**(18), 2200164 (2022)
- [24] Wang, A.Y.-T., Kauwe, S.K., Murdock, R.J., Sparks, T.D.: Compositionally restricted attention-based network for materials property predictions. *Npj Computational Materials* **7**(1), 77 (2021)
- [25] Schütt, K.T., Sauceda, H.E., Kindermans, P.-J., Tkatchenko, A., Müller, K.-R.: Schnet—a deep learning architecture for molecules and materials. *The Journal of Chemical Physics* **148**(24) (2018)
- [26] Satorras, V.G., Hoogeboom, E., Welling, M.: E (n) equivariant graph neural networks. In: *International Conference on Machine Learning*, pp. 9323–9332 (2021). PMLR
- [27] Gong, S., Yan, K., Xie, T., Shao-Horn, Y., Gomez-Bombarelli, R., Ji, S., Grossman, J.C.: Examining graph neural networks for crystal structures: limitations and opportunities for capturing periodicity. *Science Advances* **9**(45), 3245 (2023)
- [28] Goodall, R.E., Parackal, A.S., Faber, F.A., Armiento, R., Lee, A.A.: Rapid discovery of stable materials by coordinate-free coarse graining. *Science Advances* **8**(30), 4117 (2022)
- [29] Xiao, H., Li, R., Shi, X., Chen, Y., Zhu, L., Chen, X., Wang, L.: An invertible, invariant crystal representation for inverse design of solid-state materials using generative deep learning. *Nature Communications* **14**(1), 7027 (2023)
- [30] Huang, H., Magar, R., Xu, C., Farimani, A.B.: Materials informatics transformer: A language model for interpretable materials properties prediction. *arXiv preprint arXiv:2308.16259* (2023)
- [31] Fujinuma, N., DeCost, B., Hattrick-Simpers, J., Lofland, S.E.: Why big data and compute are not necessarily the path to big materials science. *Communications Materials* **3**(1), 1–9 (2022) <https://doi.org/10.1038/s43246-022-00283-x>
- [32] Bommasani, R., Hudson, D.A., Adeli, E., Altman, R.B., Arora, S., Arx, S., Bernstein, M.S., Bohg, J., Bosselut, A., Brunskill, E., Brynjolfsson, E., Buch, S., Card, D., Castellon, R., Chatterji, N.S., Chen, A.S., Creel, K., Davis, J.Q., Demszky, D., Donahue, C., Doumbouya, M., Durmus, E., Ermon, S., Etchemendy,

- J., Ethayarajh, K., Fei-Fei, L., Finn, C., Gale, T., Gillespie, L., Goel, K., Goodman, N.D., Grossman, S., Guha, N., Hashimoto, T., Henderson, P., Hewitt, J., Ho, D.E., Hong, J., Hsu, K., Huang, J., Icard, T., Jain, S., Jurafsky, D., Kalluri, P., Karamcheti, S., Keeling, G., Khani, F., Khattab, O., Koh, P.W., Krass, M.S., Krishna, R., Kudritipudi, R., al.: On the opportunities and risks of foundation models. CoRR **abs/2108.07258** (2021) [2108.07258](#)
- [33] Vaswani, A., Shazeer, N., Parmar, N., Uszkoreit, J., Jones, L., Gomez, A.N., Kaiser, Ł., Polosukhin, I.: Attention is all you need. *Advances in neural information processing systems* **30** (2017)
 - [34] Devlin, J., Chang, M.-W., Lee, K., Toutanova, K.: Bert: Pre-training of deep bidirectional transformers for language understanding. *arXiv preprint arXiv:1810.04805* (2018)
 - [35] Brown, T.B.: Language models are few-shot learners. *arXiv preprint arXiv:2005.14165* (2020)
 - [36] Lu, W., Luu, R.K., Buehler, M.J.: Fine-tuning large language models for domain adaptation: Exploration of training strategies, scaling, model merging and synergistic capabilities. *npj Computational Materials* **11**(1), 84 (2025)
 - [37] Kaplan, J., McCandlish, S., Henighan, T., Brown, T.B., Chess, B., Child, R., Gray, S., Radford, A., Wu, J., Amodei, D.: Scaling laws for neural language models. *arXiv preprint arXiv:2001.08361* (2020)
 - [38] Hoffmann, J., Borgeaud, S., Mensch, A., Buchatskaya, E., Cai, T., Rutherford, E., Casas, D.d.L., Hendricks, L.A., Welbl, J., Clark, A., et al.: Training compute-optimal large language models. *arXiv preprint arXiv:2203.15556* (2022)
 - [39] Nayak, A.K., Varshney, L.R.: An information theory of compute-optimal size scaling, emergence, and plateaus in language models. *arXiv preprint arXiv:2410.01243* (2024)
 - [40] Frey, N.C., Soklaski, R., Axelrod, S., Samsi, S., Gomez-Bombarelli, R., Coley, C.W., Gadepally, V.: Neural scaling of deep chemical models. *Nature Machine Intelligence* **5**(11), 1297–1305 (2023)
 - [41] Merchant, A., Batzner, S., Schoenholz, S.S., Aykol, M., Cheon, G., Cubuk, E.D.: Scaling deep learning for materials discovery. *Nature*, 1–6 (2023)
 - [42] Antunes, L.M., Butler, K.T., Grau-Crespo, R.: Crystal structure generation with autoregressive large language modeling. *arXiv preprint arXiv:2307.04340* (2023)
 - [43] Gruver, N., Sriram, A., Madotto, A., Wilson, A.G., Zitnick, C.L., Ulissi, Z.: Fine-tuned language models generate stable inorganic materials as text. *arXiv preprint arXiv:2402.04379* (2024)

- [44] Chithrananda, S., Grand, G., Ramsundar, B.: Chemberta: Large-scale self-supervised pretraining for molecular property prediction. CoRR **abs/2010.09885** (2020) [2010.09885](#)
- [45] Ross, J., Belgodere, B., Chenthamarakshan, V., Padhi, I., Mroueh, Y., Das, P.: Large-scale chemical language representations capture molecular structure and properties. *Nature Machine Intelligence* **4**(12), 1256–1264 (2022)
- [46] Chen, D., Zhu, Y., Zhang, J., Du, Y., Li, Z., Liu, Q., Wu, S., Wang, L.: Uncovering neural scaling laws in molecular representation learning. *Advances in Neural Information Processing Systems* **36**, 1452–1475 (2023)
- [47] Huang, H., Barati Farimani, A.: Multimodal learning of heat capacity based on transformers and crystallography pretraining. *Journal of Applied Physics* **135**(16) (2024)
- [48] Gurunathan, R., Choudhary, K., Tavazza, F.: Rapid prediction of phonon structure and properties using the atomistic line graph neural network (alignn). *Physical Review Materials* **7**(2), 023803 (2023)
- [49] Zhu, S., Ramsundar, B., Annevelink, E., Lin, H., Dave, A., Guan, P.-W., Gering, K., Viswanathan, V.: Differentiable modeling and optimization of non-aqueous li-based battery electrolyte solutions using geometric deep learning. *Nature Communications* **15**(1), 8649 (2024)
- [50] Guan, P.-W.: Differentiable thermodynamic modeling. *Scripta Materialia* **207**, 114217 (2022)
- [51] Dold, D., Egmond, D.A.: Differentiable graph-structured models for inverse design of lattice materials. *Cell Reports Physical Science* **4**(10) (2023)
- [52] Al Hassanieh, S., Reinhart, W.F., Beese, A.M.: Efficient material model parameter optimization in finite element analysis with differentiable physics. *Computational Materials Science* **253**, 113828 (2025)
- [53] Evans, M.L., Bergsma, J., Merkys, A., Andersen, C.W., Andersson, O.B., Beltrán, D., Blokhin, E., Boland, T.M., Balderas, R.C., Choudhary, K., *et al.*: Developments and applications of the optimade api for materials discovery, design, and data exchange. *Digital Discovery* **3**(8), 1509–1533 (2024)
- [54] Kittel, C., McEuen, P.: *Introduction to Solid State Physics*. John Wiley & Sons, Hoboken (2018)
- [55] Malgrange, C., Ricolleau, C., Schlenker, M.: *Symmetry and Physical Properties of Crystals*. Springer, Dordrecht (2014)
- [56] Batatia, I., Kovacs, D.P., Simm, G., Ortner, C., Csányi, G.: Mace: Higher order

- equivariant message passing neural networks for fast and accurate force fields. *Advances in Neural Information Processing Systems* **35**, 11423–11436 (2022)
- [57] Liao, Y.-L., Wood, B., Das, A., Smidt, T.: Equiformerv2: Improved equivariant transformer for scaling to higher-degree representations. *arXiv preprint arXiv:2306.12059* (2023)
 - [58] Yan, K., Fu, C., Qian, X., Qian, X., Ji, S.: Complete and efficient graph transformers for crystal material property prediction. *arXiv preprint arXiv:2403.11857* (2024)
 - [59] Jiao, R., Huang, W., Liu, Y., Zhao, D., Liu, Y.: Space group constrained crystal generation. *arXiv preprint arXiv:2402.03992* (2024)
 - [60] De Graef, M., McHenry, M.E.: *Structure of Materials: an Introduction to Crystallography, Diffraction and Symmetry*. Cambridge University Press, Cambridge (2012)
 - [61] Wyckoff, R.W.G.: *The Analytical Expression of the Results of the Theory of Space-groups* vol. 318. Carnegie institution of Washington, Washington, D.C. (1922)
 - [62] Salazar, J., Liang, D., Nguyen, T.Q., Kirchhoff, K.: Masked language model scoring. *arXiv preprint arXiv:1910.14659* (2019)
 - [63] Bao, H., Dong, L., Wei, F., Wang, W., Yang, N., Liu, X., Wang, Y., Gao, J., Piao, S., Zhou, M., *et al.*: Unilmv2: Pseudo-masked language models for unified language model pre-training. In: *International Conference on Machine Learning*, pp. 642–652 (2020). PMLR
 - [64] Yang, Z., Yang, Y., Cer, D., Law, J., Darve, E.: Universal sentence representation learning with conditional masked language model. *arXiv preprint arXiv:2012.14388* (2020)
 - [65] Dunn, A., Wang, Q., Ganose, A., Dopp, D., Jain, A.: Benchmarking materials property prediction methods: the matbench test set and automatminer reference algorithm. *npj Computational Materials* **6**(1), 138 (2020)
 - [66] Riebesell, J., Goodall, R.E., Jain, A., Benner, P., Persson, K.A., Lee, A.A.: Matbench discovery—an evaluation framework for machine learning crystal stability prediction. *arXiv preprint arXiv:2308.14920* (2023)
 - [67] Jain, A., Ong, S.P., Hautier, G., Chen, W., Richards, W.D., Dacek, S., Cholia, S., Gunter, D., Skinner, D., Ceder, G., *et al.*: Commentary: The materials project: A materials genome approach to accelerating materials innovation. *APL materials* **1**(1) (2013)

- [68] Wang, H.-C., Botti, S., Marques, M.A.: Predicting stable crystalline compounds using chemical similarity. *npj Computational Materials* **7**(1), 12 (2021)
- [69] Chen, C., Ye, W., Zuo, Y., Zheng, C., Ong, S.P.: Graph networks as a universal machine learning framework for molecules and crystals. *Chemistry of Materials* **31**(9), 3564–3572 (2019)
- [70] Wang, H., Sun, J., Liang, J., Zhai, L., Tang, Z., Li, Z., Zhai, W., Wang, X., Gao, W., Gong, S.: Crystograph: A comprehensive predictive model for crystal material properties and the benchmark. *Battery Energy*, 70004 (2024)
- [71] Abnar, S., Zuidema, W.: Quantifying attention flow in transformers. *arXiv preprint arXiv:2005.00928* (2020)
- [72] Nocedal, J.: Updating quasi-newton matrices with limited storage. *Mathematics of computation* **35**(151), 773–782 (1980)
- [73] Wang, Y., Cho, K.: Non-convolutional graph neural networks. *arXiv preprint arXiv:2408.00165* (2024)
- [74] Cai, C., Wang, Y.: A note on over-smoothing for graph neural networks. *arXiv preprint arXiv:2006.13318* (2020)
- [75] Rusch, T.K., Bronstein, M.M., Mishra, S.: A survey on oversmoothing in graph neural networks. *arXiv preprint arXiv:2303.10993* (2023)
- [76] Alon, U., Yahav, E.: On the bottleneck of graph neural networks and its practical implications. *arXiv preprint arXiv:2006.05205* (2020)
- [77] Topping, J., Di Giovanni, F., Chamberlain, B.P., Dong, X., Bronstein, M.M.: Understanding over-squashing and bottlenecks on graphs via curvature. *arXiv preprint arXiv:2111.14522* (2021)
- [78] Ward, L., Agrawal, A., Choudhary, A., Wolverton, C.: A general-purpose machine learning framework for predicting properties of inorganic materials. *npj Computational Materials* **2**(1), 1–7 (2016)
- [79] Furukawa, G.T., Douglas, T.B., McCoskey, R.E., Ginnings, D.C.: Thermal properties of aluminum oxide from 0 to 1200 k. *Journal of research of the National Bureau of Standards* **57**(2), 67–82 (1956)
- [80] Stull, D.R.: JANAF Thermochemical Tables... vol. 1. Clearinghouse, Washington, D.C. (1965)
- [81] Woodfield, B.F., Shapiro, J.L., Stevens, R., Boerio-Goates, J., Putnam, R.L., Helean, K.B., Navrotsky, A.: Molar heat capacity and thermodynamic functions for CaTiO_3 . *The Journal of Chemical Thermodynamics* **31**(12), 1573–1583 (1999)

- [82] Leitner, J., Strejc, A., Sedmidubský, D., Ruzicka, K.: High temperature enthalpy and heat capacity of gan. *Thermochimica acta* **401**(2), 169–173 (2003)
- [83] Loew, A., Sun, D., Wang, H.-C., Botti, S., Marques, M.A.: Universal machine learning interatomic potentials are ready for phonons. *arXiv preprint arXiv:2412.16551* (2024)
- [84] Leitner, J., Voňka, P., Sedmidubský, D., Svoboda, P.: Application of neumann–kopp rule for the estimation of heat capacity of mixed oxides. *Thermochimica Acta* **497**(1-2), 7–13 (2010)
- [85] Mostafa, A.G., Eakman, J.M., Montoya, M.M., Yarbrow, S.L.: Prediction of heat capacities of solid inorganic salts from group contributions. *Industrial & engineering chemistry research* **35**(1), 343–348 (1996)
- [86] Ong, S.P., Richards, W.D., Jain, A., Hautier, G., Kocher, M., Cholia, S., Gunter, D., Chevrier, V.L., Persson, K.A., Ceder, G.: Python materials genomics (pymatgen): A robust, open-source python library for materials analysis. *Computational Materials Science* **68**, 314–319 (2013)
- [87] Esters, M., Oses, C., Divilov, S., Eckert, H., Friedrich, R., Hicks, D., Mehl, M.J., Rose, F., Smolyanyuk, A., Calzolari, A., *et al.*: aflow.org: A web ecosystem of databases, software and tools. *Computational Materials Science* **216**, 111808 (2023)
- [88] Schmidt, J., Pettersson, L., Verdozzi, C., Botti, S., Marques, M.A.: Crystal graph attention networks for the prediction of stable materials. *Science advances* **7**(49), 7948 (2021)
- [89] Gjerding, M.N., Taghizadeh, A., Rasmussen, A., Ali, S., Bertoldo, F., Deilmann, T., Knøsgaard, N.R., Kruse, M., Larsen, A.H., Manti, S., *et al.*: Recent progress of the computational 2d materials database (c2db). *2D Materials* **8**(4), 044002 (2021)
- [90] Gražulis, S., Daškevič, A., Merkys, A., Chateigner, D., Lutterotti, L., Quiros, M., Serebryanaya, N.R., Moeck, P., Downs, R.T., Le Bail, A.: Crystallography open database (cod): an open-access collection of crystal structures and platform for world-wide collaboration. *Nucleic acids research* **40**(D1), 420–427 (2012)
- [91] Choudhary, K., Garrity, K.F., Reid, A.C., DeCost, B., Biacchi, A.J., Hight Walker, A.R., Trautt, Z., Hattrick-Simpers, J., Kusne, A.G., Centrone, A., *et al.*: The joint automated repository for various integrated simulations (jarvis) for data-driven materials design. *npj computational materials* **6**(1), 173 (2020)
- [92] Talirz, L., Kumbhar, S., Passaro, E., Yakutovich, A.V., Granata, V., Gargiulo, F., Borelli, M., Uhrin, M., Huber, S.P., Zoupanos, S., *et al.*: Materials cloud, a platform for open computational science. *Scientific data* **7**(1), 299 (2020)

- [93] Team, M.: Pauling File: Inorganic Materials Database. <https://paulingfile.com/>. Accessed: 2024-09-04 (2024)
- [94] Krajewski, A.M., Siegel, J.W., Liu, Z.-K.: Efficient structure-informed featurization and property prediction of ordered, dilute, and random atomic structures. arXiv preprint arXiv:2404.02849 (2024)
- [95] Fuentes-Cobas, L.E., Chateigner, D., Fuentes-Montero, M.E., Pepponi, G., Grazulis, S.: The representation of coupling interactions in the material properties open database (mpod). *Advances in Applied Ceramics* **116**(8), 428–433 (2017)
- [96] Draxl, C., Scheffler, M.: Nomad: The fair concept for big data-driven materials science. *Mrs Bulletin* **43**(9), 676–682 (2018)
- [97] Evans, M.L., Morris, A.J.: matador: a python library for analysing, curating and performing high-throughput density-functional theory calculations. *Journal of Open Source Software* **5**(54), 2563 (2020)
- [98] Armiento, R.: Database-driven high-throughput calculations and machine learning models for materials design. *Machine Learning Meets Quantum Physics*, 377–395 (2020)
- [99] Saal, J.E., Kirklin, S., Aykol, M., Meredig, B., Wolverton, C.: Materials design and discovery with high-throughput density functional theory: the open quantum materials database (oqmd). *Jom* **65**, 1501–1509 (2013)
- [100] Grygorenko, O.O., Radchenko, D.S., Dziuba, I., Chuprina, A., Gubina, K.E., Moroz, Y.S.: Generating multibillion chemical space of readily accessible screening compounds. *iScience* **23**(11), 101681 (2020) <https://doi.org/10.1016/j.isci.2020.101681>
- [101] Bellmann, L., Penner, P., Gastreich, M., Rarey, M.: Comparison of combinatorial fragment spaces and its application to ultralarge make-on-demand compound catalogs. *Journal of Chemical Information and Modeling* **62**(3), 553–566 (2022) <https://doi.org/10.1021/acs.jcim.1c01378> <https://doi.org/10.1021/acs.jcim.1c01378>. PMID: 35050621
- [102] Patel, H., Ihlenfeldt, W.-D., Judson, P.N., Moroz, Y.S., Pevzner, Y., Peach, M.L., Delannée, V., Tarasova, N.I., Nicklaus, M.C.: Savi, in silico generation of billions of easily synthesizable compounds through expert-system type rules. *Scientific Data* (2020)
- [103] Gavezzotti, A.: Are crystal structures predictable? *Accounts of chemical research* **27**(10), 309–314 (1994)
- [104] Zeni, C., Pinsler, R., Zügner, D., Fowler, A., Horton, M., Fu, X., Shysheya, S.,

- Crabbé, J., Sun, L., Smith, J., et al.: Mattergen: a generative model for inorganic materials design. arXiv preprint arXiv:2312.03687 (2023)
- [105] Barroso-Luque, L., Shuaibi, M., Fu, X., Wood, B.M., Dzamba, M., Gao, M., Rizvi, A., Zitnick, C.L., Ulissi, Z.W.: Open materials 2024 (omat24) inorganic materials dataset and models. arXiv preprint arXiv:2410.12771 (2024)
 - [106] Deng, B., Zhong, P., Jun, K., Riebesell, J., Han, K., Bartel, C.J., Ceder, G.: Chgnet as a pretrained universal neural network potential for charge-informed atomistic modelling. *Nature Machine Intelligence* **5**(9), 1031–1041 (2023)
 - [107] Park, Y., Kim, J., Hwang, S., Han, S.: Scalable parallel algorithm for graph neural network interatomic potentials in molecular dynamics simulations. *Journal of Chemical Theory and Computation* (2024)
 - [108] Chen, C., Ong, S.P.: A universal graph deep learning interatomic potential for the periodic table. *Nature Computational Science* **2**(11), 718–728 (2022)
 - [109] Gibson, J., Hire, A., Hennig, R.G.: Data-augmentation for graph neural network learning of the relaxed energies of unrelaxed structures. *npj Computational Materials* **8**(1), 211 (2022)
 - [110] Zuo, Y., Qin, M., Chen, C., Ye, W., Li, X., Luo, J., Ong, S.P.: Accelerating materials discovery with bayesian optimization and graph deep learning. *Materials Today* **51**, 126–135 (2021)
 - [111] Ward, L., Liu, R., Krishna, A., Hegde, V.I., Agrawal, A., Choudhary, A., Wolverton, C.: Including crystal structure attributes in machine learning models of formation energies via voronoi tessellations. *Physical Review B* **96**(2), 024104 (2017)

S1 Limitations and Future Work

While CLOUD shows competitive performance in crystal representation learning and property prediction, it does encounter limitations and potential improvements for future explorations. One limitation is that our model requires a large amount of pre-training data to achieve SOTA performance in many of the downstream tasks according to the scaling law we fitted, whereas such a dataset has not yet been built. Currently, the largest crystal database we can build is the one collected from OPTIMADE which includes ~ 6.3 M unique crystal structures. Compared to molecular science in which ~ 50 billion unlabeled SMILES of molecules can be easily obtained [100–102], obtaining such a large number of crystal structures is challenging despite the large design space of crystals. Not all combinations of atoms can form valid crystal structures [103] as many potential configurations are inherently unstable or chemically incompatible. Recently, a lot of machine learning models have been proposed for crystal generation [41–43, 104], however, none of them have pushed the data size to the order of billions. Recently, OMat24 dataset [105] was released which contains over 100 million DFT calculations for solid-state materials, which is a huge contribution to the research community to advance materials science development with AI. In future work, we plan to comprehensively integrate existing datasets like OMat24 and diverse generation approaches for crystal structure generation, ranging from rule-based methods to data-driven approaches. We will examine how the expanded, synthetic dataset impacts the model performance in both pre-training scaling and downstream predictive accuracy.

Another limitation lies in the representation itself: the representation we design is built on symmetry, whereas symmetry does not capture everything. For instance, while the space group, Wyckoff positions, and stoichiometry remain unchanged during relaxation, the atomic positions and cell parameters undergo significant variations. As a result, CLOUD is unable to leverage the MPtrj dataset, which comprises over 1.5 million crystal structures from relaxation trajectories, unlike many other models on the leaderboard [66, 106]. In addition, the representation does not work for amorphous materials which lack the long-range order and symmetry that crystalline materials exhibit, thus limiting the versatility of CLOUD in handling a broader range of materials. Furthermore, some Wyckoff positions include free variables, meaning the representation encodes an ensemble of materials. As a result, it may not distinguish between materials with different physico-chemical properties that share the same prototype but have different atomic positions. In future work, we plan to systematically investigate the design of string representations for crystals which enables effective encoding of more information besides symmetry and composition, while building the multi-modal framework for crystalline materials as an alternative to incorporate comprehensive structural information.

S2 Implementation Details

S2.1 Additional Dataset Information

MatBench [65] is a benchmark test suite that contains 13 tasks using data from density functional theory-derived and experimental sources. We use 8 out of 13 tasks for benchmarking as they are regression tasks and provide the crystal structures to build the SCOPE representation.

MatBench Discovery [66] is a comprehensive resource designed to evaluate machine learning models for materials discovery, particularly for predicting the thermodynamic stability of materials. The dataset aims to reflect practical challenges in the discovery process by requiring predictions based on unrelaxed crystal structures, which avoid reliance on expensive DFT calculations. The models are trained on customized training data and tested on WBM dataset [68] which contains $\sim 257\text{K}$ OOD crystal structures generated by systematically substituting elements in pre-existing structures from the Materials Project (MP). This dataset is heavily composed of ternary phases, with a significant fraction of transition metals and metalloids, offering a broader chemical diversity than the MP dataset. The WBM is designed to challenge models to perform OOD predictions, making it a demanding benchmark for stability.

UnconvBench [70] consists of unconventional crystal structures including 2D crystals, metal-organic frameworks (MOFs), defected crystals. The benchmark contains various crystals with irregular and complex long-range, whereas such crystalline systems are rarely observed in highly ordered traditional crystals. Hence, UnconvBench provides complementary insights to existing benchmark datasets, offering a broader perspective on evaluating model performance on unconventional materials (which are in fact conventional in the real world).

C_v and U datasets [27] consist of heat capacity (C_v) and phonon internal energy (U) data for a diverse set of materials. The dataset is derived from DFT calculations and provides key thermodynamic properties at 300K. The phonon properties heavily depend on the periodicity and bonding strength of the crystal structure, making this dataset a crucial benchmark for evaluating machine learning models’ ability to capture long-range interactions and structural periodicity. The dataset has been used in previous studies to analyze the limitations of graph neural networks in predicting phonon-related properties and has been shown to benefit from explicit periodicity encoding.

S2.2 Training Details

The hyperparameters used for training CLOUD are summarized in Table S1. A list of values is shown in the table if the hyperparameter takes different values for different tasks. The model architecture is fixed to 12 hidden layers and 12 attention heads in each layer for the BERT part in CLOUD when used for benchmarking, while we experiment with smaller models in order to fit the scaling law. The number of hidden layers is fixed to 1 for experiments on MatBench for a fair comparison, while we experiment with up to 3 hidden layers in the prediction head on MatBench Discovery

Table S1 Hyperparameters of CLOUD.

Hyperparameter	Value
# of hidden layers in BERT	{1,3,6,12}
# of attention heads in BERT	{1,4,12}
# of hidden layers in MLP	{1,2,3}
max position embeddings	64
block size	64
embedding size	768
# of hidden layers in MLP	{1,2,3}
hidden layer width in MLP	768
activation function in MLP	SiLU
pre-train epochs	50
pre-train learning rate	1e-4
pre-train batch size	2048
pre-train weight decay	0.0
pre-train optimizer	AdamW
pre-train scheduler	linear warmup and cosine decay
pre-train warm-up ratio	0.05
fine-tune epochs	{50,100,200}
fine-tune learning rate	{1e-4,5e-5}
fine-tune batch size	{32,64,128,512}
fine-tune weight decay	{0.0, 0.0001, 0.01}
fine-tune optimizer	AdamW
fine-tune scheduler	linear warmup and cosine decay
fine-tune warm-up ratio	{0.05,0.1}
fine-tune # of freezing-encoder epochs	{0,5,10}

and UnconvBench for optimal performance as we do not need to compare with MatInFormer or SLICES-BERT on those two benchmarks. The hyperparameters that are used in experiments for pre-training and fine-tuning are also listed in Table S1.

S2.3 Baseline

We summarize the baseline models used for benchmarking in Table S2. The baselines cover a variety of models:

- Voronoi RF directly uses chemical descriptors as features for input.
- Roost, Finder, and CrabNet use composition only as input.
- coGN, coNGN, ALIGNN, MEGNet, CGCNN, CGCNN+P, and BOWSR build graphs from crystal structures and learn the mapping from the structure to target properties.
- SevenNet, MACE, CHGNet, and M3GNet are GNNs trained to serve as universal machine learning-based interatomic potentials (MLIPs).
- CrysToGraph is a transformer-based geographic model for learning both local and long-range information from graphs.
- MatInFormer, Wrenformer, and SLICES-BERT are built on a transformer architecture and take sequences as input, same as our model CLOUD.

Table S2 Summary of baseline models used in this work.

Model	Type	Architecture	Source
coGN	Structure-based	GNN	[22]
coNGN	Structure-based	GNN	[22]
ALIGNN	Structure-based	GNN	[21]
CGCNN	Structure-based	GNN	[19]
CrabNet	Structure-agnostic	Transformer	[24]
Finder	Structure-agnostic	GNN	[23]
Roost	Structure-agnostic	GNN	[20]
Wrenformer	Coordinate-free	Transformer	[66]
MatInFormer	Coordinate-free	Transformer	[30]
SLICES-BERT	Coordinate-free	Transformer	[29]
SevenNet	Structure-based (MLIP)	GNN	[107]
MACE	Structure-based (MLIP)	GNN	[56]
CHGNet	Structure-based (MLIP)	GNN	[106]
M3GNet	Structure-based (MLIP)	GNN	[108]
MEGNet	Structure-based	GNN	[69]
CGCNN+P	Structure-based	GNN	[109]
BOWSR	Structure-based	GNN	[110]
Voronoi RF	Feature-based	Random Forest	[111]
CrysToGraph	Structure-based	Graph Transformer	[70]

S2.4 Evaluation Metrics

Our evaluation strategies follow the ones adopted by the benchmark leaderboards. We use MAE as the metric for regression tasks in MatBench and UnconvBench. MatBench Discovery leaderboard provides results for multiple metrics: MAE, RMSE, and R^2 for energy above convex hull prediction, and F1, accuracy, precision, true positive rate (TPR), and true negative rate (TNR) for stability classification. In particular, [66] propose discovery acceleration factors (DAF) quantifies how much faster a machine learning model can identify stable materials compared to random selection. The expression of DAF is given as follows:

$$DAF = \frac{Precision}{N_{stable,true}/N_{total}} \quad (19)$$

where $N_{stable,true}$ and N_{total} are the number of stable materials and the total number of materials in the dataset, respectively.

We also provide the results for ROC-AUC in order to remove the sensitivity of the classification metrics to the choice of thresholds.

For C_v and U datasets, we use MAE/MAD as the metric, consistent with the original literature [27]. First proposed in [21], the metric normalizes MAE with the mean absolute deviation (MAD) so that model performance could be compared across datasets with different units and scales:

$$MAE/MAD = \frac{\sum |y_i - y_{i,true}|}{\sum |y_{i,true} - \bar{y}|} \quad (20)$$

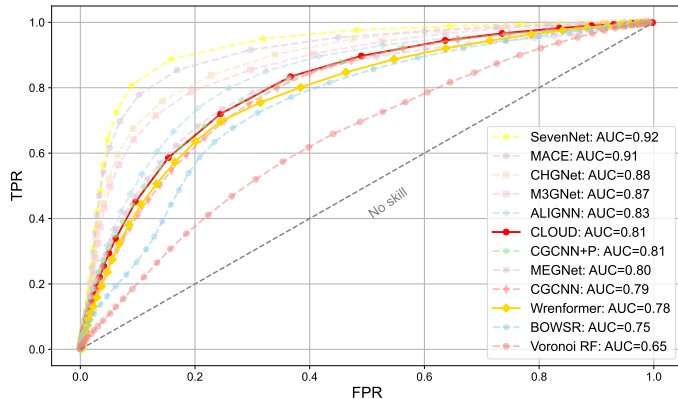


Fig. S1 Receiver operating characteristic (ROC) curves for each model evaluated on MatBench Discovery. False positive rate (FPR) on the x-axis is the fraction of unstable structures classified as stable. True positive rate (TPR) on the y-axis is the fraction of stable structures classified as stable. Area under curve (AUC) scores are calculated and presented in descending order. More models are included in the plot compared to Figure 2c.

where y_i and $y_{i,true}$ are the predicted value and the true value of the i th data point, and \bar{y} is the mean of the true values in the dataset. Usually, a model will be considered as a good predictive model if $MAE/MAD < 0.2$ [21, 78].

S3 Additional Results

S3.1 MatBench

We provide the MAE for each model on the eight regression tasks from MatBench [65] in Table S3. We provide the average MAE as well as the standard deviation on five folds for each task. CLOUD surpasses all the other structure-agnostic and coordinate-free models on 7 out of 8 tasks on MatBench. Furthermore, CLOUD achieves state-of-the-art results on jdft2d and dielectric datasets.

S3.2 MatBench Discovery

We train the model on Materials Project [67] formation energy data from the v2022.10.28 MP release, then make predictions for the unrelated structures in the WBM dataset [68] which are generated via elemental substitution of MP source structures so that the generated structures are not included in the training set. When evaluating the models on MatBench Discovery, we record the classification results under varied thresholds and plot the receiver operating characteristic (ROC) curve for CLOUD and the major structure-based models that are trained on MatBench. We plot the ROC curves with more models included in Figure S1 compared to Figure 2c. Though not comparable to machine-learned interatomic potentials (MLIPs) at this stage, CLOUD still shows solid performance compared with CGCNN, MEGNet, Wrenformer, etc.

We further examine the other metrics listed in Table S4. The regression metrics of CLOUD are again second to ALIGNN while outperforming CGCNN and MEGNet. The classification metrics for CLOUD are close to those of Wrenformer under the stability threshold of 0, as shown in Table S4.

Table S3 Results on MatBench regression tasks. All results are shown in the mean of test MAE in five-fold cross-validation along with the standard deviation in brackets. The best and the second best results among structure-agnostic and coordinate-free models are in bold and underlined, and the best results among all the models are in italics.

Model	jdf2d (↓)	phonons (↓)	dielectric (↓)	gvrh (↓)	kvth (↓)	perovskites (↓)	band gap (↓)	e form (↓)
coGN	37.1652 (13.6825)	29.7117 (1.9968)	0.3088 (0.0859)	0.0689 (0.0009)	0.0535 (0.0028)	<i>0.0969 (0.0008)</i>	<i>0.1559 (0.0017)</i>	<i>0.0170 (0.0003)</i>
coNGN	36.1698 (11.5973)	<i>28.8874 (3.2840)</i>	0.3142 (0.0740)	<i>0.0670 (0.0006)</i>	<i>0.0491 (0.0026)</i>	0.0290 (0.0011)	0.1697 (0.0035)	0.0178 (0.0004)
ALIGNN	43.4244 (8.9491)	29.5385 (2.1148)	0.3449 (0.0871)	0.0715 (0.0006)	0.0568 (0.0028)	0.0288 (0.0009)	0.1861 (0.0030)	0.0215 (0.0005)
CGCNN	49.2440 (11.5865)	57.7635 (12.3109)	0.5988 (0.0833)	0.0895 (0.0016)	0.0712 (0.0028)	0.0452 (0.0007)	0.2972 (0.0035)	0.0337 (0.0006)
CrabNet	45.6104 (12.2491)	55.1114 (5.7317)	0.3234 (0.0714)	0.1014 (0.0017)	0.0758 (0.0034)	0.4065 (0.0069)	0.2655 (0.0029)	0.0862 (0.0010)
Finder	47.9614 (11.6681)	46.5751 (3.7415)	0.3204 (0.0811)	0.0996 (0.0018)	0.0764 (0.0025)	0.6450 (0.0167)	0.2308 (0.0029)	0.0839 (0.0011)
Roost	44.6405 (11.7353)	54.3893 (4.7283)	0.3252 (0.0780)	0.1034 (0.0020)	0.0797 (0.0042)	0.4025 (0.0077)	0.2571 (0.0055)	0.0847 (0.0016)
Wrenformer	39.6309	92.3349	0.3583	0.1070	0.0811	0.3351	0.2986	0.0694
MatInFormer	45.1309 (12.7339)	44.0134 (5.7265)	0.3046 (0.0765)	0.0873 (0.0019)	0.0703 (0.0030)	0.4339 (0.0105)	0.2541 (0.0020)	0.0646 (0.0003)
SLICES-BERT	37.8586 (10.9928)	44.5470 (4.0192)	0.3417 (0.0918)	0.0932 (0.0015)	0.0698 (0.0021)	0.0351 (0.0013)	0.2776 (0.0043)	0.0543 (0.0004)
CLOUD	<i>35.0037 (11.4390)</i>	40.6856 (2.6168)	<i>0.3038 (0.0782)</i>	0.0873 (0.0028)	0.0682 (0.0026)	0.0969 (0.0010)	0.2126 (0.0030)	0.0542 (0.0007)

Table S4 Classification and regression metrics for models tested on MatBench Discovery ranked by F1 score. The stability threshold for model predictions are set to 0.

Model	F1 (↑)	DAF (↑)	Prec (↑)	Acc (↑)	TPR (↑)	TNR (↑)	MAE (↓)	RMSE (↓)	R^2 (↓)
SevenNet	0.719	3.804	0.653	0.893	0.800	0.912	0.046	0.090	0.750
MAE	0.668	3.400	0.583	0.867	0.781	0.885	0.055	0.099	0.698
CHGNet	0.612	3.038	0.521	0.839	0.740	0.859	0.061	0.100	0.690
M3GNet	0.576	2.647	0.454	0.802	0.788	0.804	0.072	0.115	0.588
ALIGNN	0.565	2.921	0.501	0.829	0.649	0.866	0.092	0.154	0.274
MEGNet	0.513	2.699	0.463	0.813	0.574	0.862	0.128	0.204	-0.277
CGCNN	0.510	2.631	0.451	0.807	0.587	0.852	0.135	0.229	-0.624
CGCNN+P	0.510	2.398	0.411	0.779	0.670	0.801	0.108	0.178	0.027
Wrenformer	0.479	2.130	0.365	0.741	0.693	0.751	0.105	0.182	-0.020
CLOUD	0.474	2.043	0.340	0.711	0.781	0.697	0.104	0.167	0.147
BOWSR	0.437	1.836	0.315	0.702	0.711	0.680	0.114	0.164	0.142
Voronoi RF	0.344	1.509	0.259	0.665	0.511	0.697	0.141	0.206	-0.316
Dummy	0.194	1	0.168	0.680	0.231	0.770	0.120	0.181	0

Table S5 Classification metrics for CLOUD tested on MatBench Discovery under varying stability thresholds.

Threshold	F1 (\uparrow)	DAF (\uparrow)	Prec (\uparrow)	Acc (\uparrow)	TPR (\uparrow)	TNR (\uparrow)
-0.05	0.467	2.903	0.484	0.828	0.451	0.904
0.0	0.474	2.043	0.340	0.711	0.781	0.697
0.05	0.380	1.434	0.239	0.494	0.932	0.407

We list the classification results by CLOUD under different stability thresholds in Table S5. Note that the true labels for the test data are derived with the threshold of 0, consistent with the benchmark setting [66], while the dynamic threshold applies to the model prediction. More negative thresholds will result in higher precision for CLOUD and subsequently higher DAF, which is also observed for models that are more optimistic in stability predictions like CHGNet [66]. However, the trade-off across metrics leads to decreased F1 score and TPR when a negative threshold is used.

S3.3 UnconvBench

Table S6 summarizes the model performance in terms of MAE on UnconvBench to evaluate the predictive performance for ‘unconventional’ crystals, which are in fact the prevailing crystals in the real world. We provide the average MAE as well as the standard deviation on five folds for each task. CLOUD demonstrates comparable performance to the SOTA model CrysToGraph and significantly outperforms the other structure-based models.

Table S6 Results on UnconvBench general predictive tasks. All results are shown in the mean of test MAE in five-fold cross-validation. The best results are in bold and the second-best results are underlined. The standard deviations are shown in brackets.

Type	Model	2d_e.exf (\downarrow)	2d_e.tot (\downarrow)	2d_gap (\downarrow)	qnoF (\downarrow)	supercon (\downarrow)	defected (\downarrow)
Structure-based	CrysToGraph	0.0500 (0.0016)	0.3623 (0.0210)	0.0986 (0.0117)	121.9662 (2.001)	2.6422 (0.1722)	0.8885 (0.1641)
	coGN	0.0510 (0.0020)	0.5214 (0.1278)	0.1168 (0.0178)	218.9272 (10.640)	2.8955 (0.1522)	1.0615 (0.1268)
	coNGN	0.0530 (0.0026)	0.4497 (0.1091)	0.1432 (0.0197)	229.1948 (12.468)	2.9167 (0.0940)	1.0441 (0.1539)
	ALIGNN	0.0580 (0.0031)	0.3705 (0.0743)	0.1048 (0.0145)	217.2508 (6.738)	2.7372 (0.1069)	0.9842 (0.1325)
Coordinate-free	CGCNN	0.0710 (0.0053)	1.2941 (0.1208)	0.1499 (0.0209)	231.1887 (8.2983)	2.9316 (0.1069)	1.1321 (0.1100)
	CLOUD	0.0569 (0.0054)	0.3723 (0.0286)	0.0919 (0.0070)	159.5723 (9.6317)	2.6925 (0.1337)	0.8197 (0.1093)

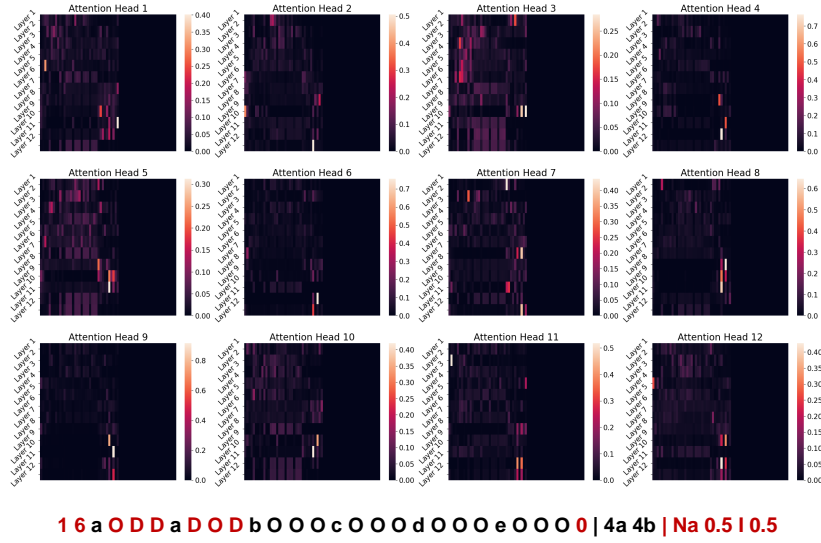


Fig. S2 Visualization of the attention scores between the [CLS] token and the other tokens in different hidden layers and attention heads for NaI example from the C_v test set. The corresponding string representation is put under the plot with the tokens of high attention scores marked in red.

S3.4 Attention Visualization

We visualize the attention score between the [CLS] token and the other tokens in SCOPE from different hidden layers and attention heads in Figure S2, using NaI from the C_v dataset as an example. While [CLS] tends to attend to different tokens in different attention heads, which is expected as different attention heads are meant to capture features in different subspaces, some tokens are intensively attended across attention heads which are highlighted in red at the bottom of the figure. Aside from material compositions, space group tokens also have relatively high attention scores with [CLS], which partly explains why CLOUD exceeds GNNs in learning features of global crystal structures and achieving high accuracy in predicting heat capacity and phonon internal energy.